ELSEVIER

Marine Geology 208 (2004) 43–72

MARINE GEOLOGY
INTERNATIONAL JOURNAL OF MARINE GEOLOGY, GEOCHEMISTRY AND GEOPHYSICS

www.elsevier.com/locate/margeo

Tracer studies on the updrift margin of a complex inlet system

Ana Vila-Concejo[a,*], Óscar Ferreira[b], Paolo Ciavola[c], Ana Matias[a], João M.A. Dias[b]

[a] CIACOMAR/CIMA, Universidade do Algarve, Avenida 16 de Junho s/n, 8700-311 Olhão, Portugal
[b] FCMA/CIMA, Universidade do Algarve, Campus de Gambelas s/n, 8000 Faro, Portugal
[c] Dipartimento di Scienze della Terra, Univ. Ferrara, Corso Ercole I d'Este, 32, Ferrara 44100, Italy

Received 31 January 2003; received in revised form 5 February 2004; accepted 28 April 2004

Abstract

Three sediment transport studies using tracers were performed at Ancão Inlet (southern Portugal). The objectives of the experiments were to understand the sediment transport pathways and to determine their magnitudes on the updrift margin of an inlet. In order to apply the traditionally used Space Integration Methodology to the tracer experiments, adaptations were required. The study area was divided into four morphologically defined sectors and this was found to be a key factor for the applicability of tracers in a complex area. The four sectors are as follows: sector A is the straight part of the updrift beach; sector B is the upper area of the swash platform; sector C is the lower area of the swash platform; and sector D represents the inner parts of the inlet margin. The integrated analysis of all collected data (forcing mechanisms, tracer distribution and topographic evolution) led to the determination of the sediment pathways. A semi-quantitative conceptual model was developed in order to explain the sediment transport pathways and magnitudes that a known mass of sediment would follow after arriving at the swash platform. It was found that the areas with the largest sediment accumulation were sectors B and C, while almost no sediment was retained in sector D, which experienced significant erosion. According to the model, 53% of the initial mass of sediments remain in the system after two tidal cycles. It is hypothesised that sediment losses are caused by sediment transport towards the ebb delta and by sediment bypassing occurring from the ebb delta to the downdrift beach through swash bar processes. The herein defined conceptual model represents a useful tool that could be applied to other tidal inlets under similar conditions, facilitating sediment budget studies around tidal inlets.

Keywords: tidal inlet; fluorescent tracers; swash platform; sediment transport; Ancão; Portugal

1. Introduction

Tidal inlets in barrier island systems represent some of the most dynamic features of the world's coastlines and, consequently, they have been the subject of many investigations. Inlet studies are motivated by a need for improving the knowledge of natural and artificial inlet evolution and behaviour (i.e., Nummedal and Fisher, 1978; Hicks and Hume, 1997; Williams et al., 1998, 2003; Morang, 1999; FitzGerald et al., 2001; Morris et al., 2001, 2004), because a large number of inlets have direct and indirect impacts on regional economy. Natural and anthropogenic factors such as sea level rise, storms, dune occupation or coastal engineering interventions often produce changes in tidal inlet conditions. Thus engineering interventions including inlet

* Corresponding author. Tel.: +351-289-707-087; fax: +351-289-706-972.
E-mail address: aconcejo@ualg.pt (A. Vila-Concejo).

0025-3227/$ - see front matter © 2004 Elsevier B.V. All rights reserved.
doi:10.1016/j.margeo.2004.04.020

relocation (i.e., Kana and Mason, 1988; Vila et al., 1999; Vila-Concejo et al., 2003a; 2004) or channel dredging (i.e., Johnsen et al., 1999) are often needed to maintain the efficiency of water exchange and/or navigability of tidal inlets. The study of the sediment budget in inlet areas is a key element for the successful planning and execution of any engineering interventions. According to Rosati and Kraus (1999), inlets increase the complexity of sediment budgets because sediment transport magnitudes and pathways are difficult to define because of the combined effect of tidal currents (ebb and flood), and waves over a complex bathymetry. Therefore, improving the knowledge of sediment transport inside inlet systems is needed in order to provide a better understanding of their evolution.

According to Allen (1988), sediment tracer studies apparently provide the best information on nearshore transport. Sediment tracer studies have been widely used for the study of sediment transport on straight beaches (i.e., Komar and Inman, 1970; Komar, 1977; Kraus, 1985; Kraus et al., 1982; Michel, 1997; Ciavola et al., 1997; 1998). As a consequence, some empirical formulae have been developed to calculate longshore transport (i.e., C.E.R.C., 1984; Kamphuis et al., 1986). However, sediment tracer techniques have also been applied to more complex systems such as swash platforms (Oertel, 1972), submarine sand banks (Collins et al., 1995), swash bars on swash platforms (Balouin et al., 2001) and harbours (Ferreira et al., 2002), and provided useful information on sediment transport.

This paper presents the results obtained from the application of sediment tracer studies on the updrift margin of an inlet. Some adaptations were made to the traditional techniques used in the literature and the sediment transport pathways were defined in a semi-quantitative way. This paper represents a contribution to the knowledge and understanding of sediment transport patterns on the updrift margin of mixed-energy tidal inlets. The main aim is to obtain a detailed picture of the sediment transport pathways on the updrift margin of mixed-energy tidal inlets.

2. Study area

The present study was performed at Ancão Inlet, which is located in the Ria Formosa, a multi-inlet barrier island system located in southern Portugal (Fig. 1).

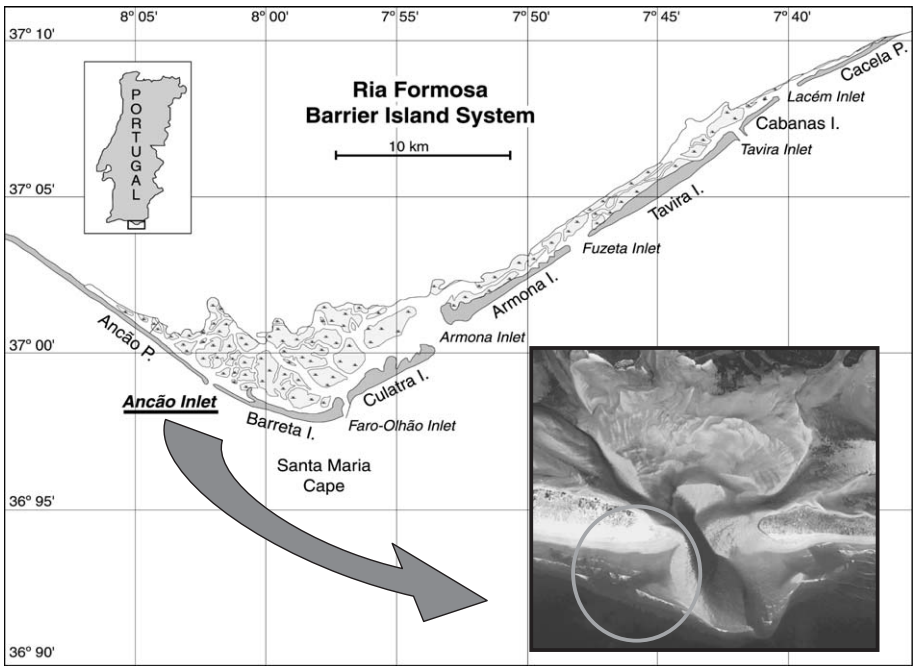

Fig. 1. Location of Ancão Inlet inside the Ria Formosa barrier island system. An aerial photo of Ancão Inlet shows its appearance on the 18th April 1999.

The Ria Formosa is a natural park that is composed of a group of five barrier islands and two peninsulas, extending for approximately 50 km from Ancão to Cacela. The backbarrier area consists mainly of salt marsh and small sandy islands, covering 8.4×10^7 m^2 and comprising a complicated pattern of tidal channels and creeks with an average depth of 4 m below mean sea level (msl) (Andrade, 1990). The origin of the Ria Formosa is not clear; however, Pilkey et al. (1989) established the historical landform migration to be in agreement with the classical shoreface transgression model (i.e., Hoyt, 1967).

Tides in the area are semi-diurnal, average ranges are 2.8 m for spring tides and 1.3 m during neap tides; however, maximum ranges of 3.5 m occur. Wave climate in the area is moderate (Ciavola et al., 1997), average values for significant wave height (H_s) and peak period (T_p) are smaller in summer ($H_s = 0.78$ m; $T_p = 7.1$ s) than in winter ($H_s = 1.15$ m; $T_p = 9.2$ s), indicating the higher frequency of swell conditions (Costa, 1994). Incident waves are most often from the west–southwest (W–SW), occurring 68% of the time, although 'Levante' (southeast, SE, Mediterranean wind) events occur often in the area, producing east–southeast (E–SE) waves 29% of the time (Costa, 1994). Storms in the study area correspond to events with H_s greater than 3 m (Pessanha and Pires, 1981). Net littoral drift and longshore currents in the area are typically from west to east (Granja et al., 1984; Consulmar, 1989 in Bettencourt, 1994; Andrade, 1990; Bettencourt, 1994). Estimates range between a minimum of 6000 m^3/year obtained by Andrade (1990), and a maximum of 300,000 m^3/year (Consulmar, 1989 in Bettencourt, 1994). These estimates vary widely mostly because of the different data sources and methods applied.

According to Vila-Concejo et al. (2002), Ancão Inlet undergoes an eastward migration cycle that lasts 30–40 years. During these cycles, the inlet migrates to the east with variable migration rates while the width of the channel at the inlet throat remains almost constant. In late 1996, Ancão Inlet was in the last stage of its migration cycle (Vila-Concejo et al., 2002). Water exchange efficiency was low due to meandering and infilling. On the basis of the soft intervention policy of the Ria Formosa Natural Park (Dias et al., 2003), a new inlet was opened on the 23rd of June 1997. Ancão Inlet reached dynamic equilibrium 1 year after its opening and has behaved like a natural inlet since that time (Vila et al., 1999; Vila-Concejo et al., 2003a, 2004).

Ancão Inlet (Fig. 1) shows characteristics of both a tidal (well-defined deep main channel and marginal flood channels) and a wave-dominated inlet (relatively small ebb delta), being tide-dominated most of the time (Morris et al., 2001). Morris et al. (2004), using video techniques, defined a conceptual model for the seasonal morphological evolution of Ancão Inlet. They defined three main morphological states that Williams et al., (2003) correlated with other studies made at the inlet. According to Morris et al. (2001, 2004) and Williams et al. (2003), most of the morphological changes at Ancão Inlet occur during storms.

3. Methods

As part of the INDIA project intensive field campaign, three experiments (AMI.1, AMI.2 and AMI.3) were planned and performed at the easternmost spit of Ancão Peninsula, on the western shore of Ancão Inlet (Fig. 1). The main objectives were to identify, understand and, when possible, quantify the sediment transport patterns and processes that were occurring on the updrift margin of Ancão Inlet. The identified processes were then analysed to develop a semi-quantitative conceptual model of the sediment paths and magnitudes. The particular objectives of each campaign are explained individually in Section 3.2 together with the setting of the experiments.

3.1. Forcing mechanisms measurement

Two biaxial electromagnetic currentmeters, EMCMo (1.6 Hz) and EMCMn (16 Hz), were hard-wired to a continuously logging PC and used in all field campaigns. For the AMI.3 campaign, the University of Ferrara deployed its RUNTI system with one biaxial electromagnetic currentmeter (EMCMr) and one pressure transducer (PTr), which were self-logging and collected data as 20-min bursts at 4 Hz every half hour.

Other data used in this study were obtained under the framework of the INDIA project (Williams et al., 1999, 2003): (1) Wind data were obtained in situ by the University of Amsterdam between the 12th of

January and the 26th March 1999; however, due to the low intensity of the recorded winds, these data were considered negligible for the present study; (2) offshore wave data were obtained from a Triaxys wave rider buoy that was temporarily deployed (between the 13th January and the 25th March) with coordinates 36°58.0′ N and 08 00.1′ W, at a depth of 25 m. Records were obtained every hour. Where there were gaps in buoy records, data were obtained from a wave-rider buoy placed by the Instituto Hidrográfico de Portugal (IH) offshore of Santa Maria Cape (Fig. 1) with coordinates 36°54.3′ N, 07°53.9′ W at a depth of 93 m. In this case records were obtained every 3 h. IH also provided predicted hourly tide elevations. For AMI.3, tide elevations were obtained every 30 min from the PTr at the RUNTI location.

3.2. Setting of the experiments

An irregular grid, defined for the study area according to the morphologic characteristics at the time (Fig. 2), was used for topographic measurements and sample collection for all of the experiments. Profiles were named according to the distance between the profile origin and a reference profile (profile 0, P0). Distance between profiles was 50 m in the straight part of the area (P0 to P400), while radial profiles were defined for the inlet margin with a spacing of 10 m between profile origins (P410 to P500). P520 to P650 were located on the inner beach, spacing between profiles was variable ranging from 10 to 50 m.

Preparation of the fluorescent tracers (FT) entailed collecting sediment from the study area, washing to eliminate salt, dying with orange fluorescent ink (Atomlac Industrie Glycero Orange Fluo), and sieving to remove aggregates (Ciavola et al., 1998). The FT were not sieved for AMI.2 and AMI.3 because of the coarse nature of the sediments on the swash platform. Before placing in the field, FT grains were washed with seawater and a small amount of detergent to lubricate the grains, to avoid the transport of the tracers as a floating layer. The sampling area was determined by

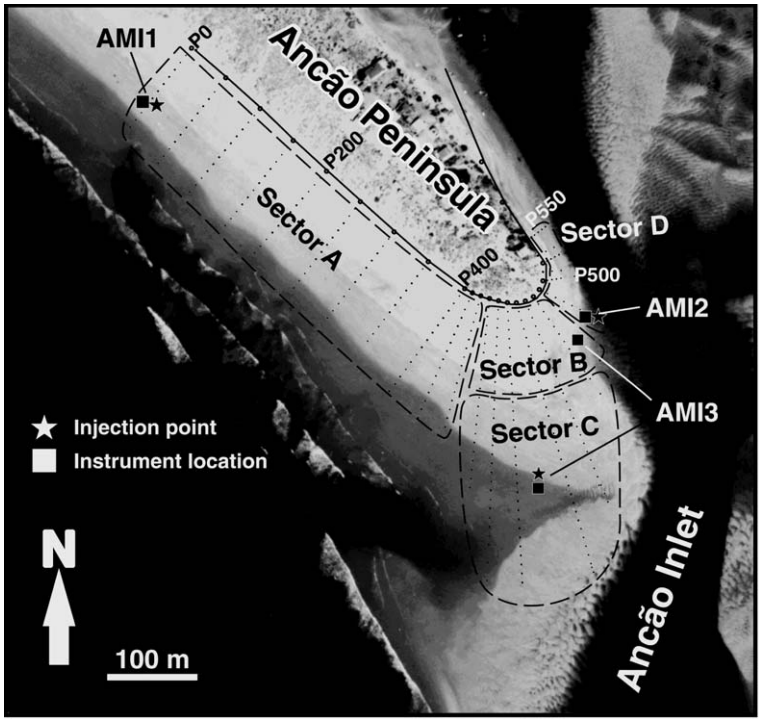

Fig. 2. Aerial photo of the study area showing the profiling/sampling grid as well as the instrument and injection locations for each campaign. Sectors dividing the study area (A, B, C and D) are also shown.

detecting the presence of FT using a portable UV light. Shore-normal spacing between samples along a profile was between 10 and 60 m, depending on the total length of the profile, the spacing being larger on the longer radial profiles located on the sand spit. Sampling was undertaken during the first and second low tides after tracer deployment. Sample collection consisted of shallow cores (~ 30–40 cm) that were then sectioned into 5 cm samples. Semi-surficial samples, using small containers of 10 cm depth, were taken in areas covered with water or when dispersion of the tracers was expected to be too high. When available, a boat was used for taking submarine samples in the adjacent areas using a Van Veen grab.

The objectives of the AMI.1 campaign were to determine the sediment transport patterns of the updrift beach and the inputs of sediment from the beach into the inlet area, quantifying the percentages of sediment either moving towards the backbarrier area or going towards the ebb-delta area. The settings of this campaign are summarised in Table 1 and Fig. 2. The FT were placed on the lower beach face on the first low tide on 20 January. The EMCMo did not acquire any data during this campaign because of technical problems. Elevations above the bed for EMCMn were 10 cm for the first recorded tide and 12.5 cm for the second one. The first low tide sampling (LTS1) was carried out at night on 20 January (AMI.1-1), corer samples were collected along the sampling grid from P0 to P420. The second low tide sampling (LTS2) was undertaken on the morning of 21 January (AMI.1-2) corer sample collection was performed between P150 and P520.

The objectives of the AMI.2 campaign were to determine the sedimentary exchange at the western edge of the inlet and the interactions with the beach, lagoon, channel, and ebb delta. The settings of this campaign are summarised in Table 1 and Fig. 2. The FT were placed on the lower part of P490 on the second low tide of 17 February. Elevations above the bed for EMCMo and EMCMn were respectively 31.5 and 34 cm for the first recorded tide and 47 and 48 cm for the second one. The LTS1 was carried out on the morning of 18 February (AMI.2-1), corer samples were collected between P430 and P520, and 22 submarine semi-surficial samples were taken from the channel and from the area located in front of the swash platform. The LTS2 was undertaken on the night of 18 February (AMI.2-2), large dispersion of the FT was expected, and thus semi-surficial samples were collected between P400 and P550.

The objectives of the AMI.3 campaign (18–20 March 1999) were to determine the sedimentary exchanges between the swash platform, the western shore of the inlet, the inlet channel and the beach. The settings of this campaign are summarised in Table 1 and Fig. 2. During the second low tide of 18 March, the FT were placed between P450 and P460 on the swash platform that connects the inlet margin with the ebb delta. Elevations above the bed for EMCMn and EMCMo were respectively 40 and 18 cm for the first recorded tide and 37 and 44 cm for the second one. The LTS1 was undertaken with cores on the morning of 19 March (AMI.3-1) between P440 and P500 and 30 submarine samples were acquired in the channel and in front of the swash platform from a boat. The LTS2 was conducted at night on 19 March between profiles P400 and P540 (AMI.3-2).

3.3. Data analyses

3.3.1. Forcing mechanisms

Wave parameters used for this study were significant wave height (H_s), peak period (T_p) and mean

Table 1
Setting of the experiments, positions and extents are referred to P0

	Date (1999)	FT mass (kg), position	Topography date and extent (low tide)	Position relative to P0 and orientation of currentmeters[a]				FT samples[b]	
				FT	EMCMo	EMCMn	RUNTI	LTS1	LTS2
AMI.1	20–22 Jan	300, P0	22 Jan, P0–P650	P0	P500 (error)	P0 (L–C)	–	418 (c)	512 (c)
AMI.2	17–19 Feb	100, P490	18 Feb, P400–P550	P490	P490 (L–V)	P490 (L–C)	–	549 (c+b)	93 (s)
AMI.3	18–20 Mar	290, P455	18 Mar, P350–P600	P455	P485 (L–C)	P485 (L–V)	P455 (L–C)	517 (c+b)	99 (s)

[a] The orientation of the currentmeters is L for longshore, C for cross-shore and V for vertical.
[b] The samples were taken as corer samples (c), semi-surficial samples (s) or from the boat (b).

wave direction at peak frequency (MWD). The *in situ* wave data obtained from the PTr during AMI.3 was processed using spectral analysis according to methods described in Ciavola (1999).

Data files from the EMCMs were filtered to eliminate high frequency peaks that could be a source of error. Average current velocities were calculated for sample bursts of 15 min for EMCMo and EMCMn, and over 30 min for EMCMr. The velocity and direction of the resultant current was calculated for every burst.

3.3.2. Topography

Linear kriging was used to interpolate topographic profiles; spacing of the interpolation nodes was adjusted as a function of the distance between measured points. The morphologic and volumetric evolution of the easternmost spit of Ancão Peninsula was obtained by comparison of these data.

Slopes were calculated for the beach face (tan β_{bf}), on profiles located on the oceanic beach, and for the swash platform (tan β_{sp}), on profiles located on the oceanic side of the inlet margin (P430 to P460). The surf scaling parameter (ϵ) (Guza and Inman, 1975) was used to define whether the profile was reflective or dissipative. The surf similarity parameter (ξ_b) (Battjes, 1974) was calculated in order to determine the breaking type of the incident waves. Breaking wave heights used for the calculation of ξ_b were obtained by visual observation.

3.3.3. Tracers

Grain-size analysis (mean and sorting) was performed in order to compare the natural sand from the study area with the FT (Folk and Ward, 1957) using the computer program GRADISTAT of Blott and Pye (2001). FT grains present in the LTS1 of AMI.1 (AMI.1-1) were manually counted under a UV lamp. An automatic system, FENIX (Vila-Concejo et al., 2003b), was developed and used for the reminder of the samples. The system was calibrated for each campaign because of differences in grain-size and shell contents. The number of FT grains for 100 g of sample was then computed in order to generate maps of tracer distribution.

The definition of FT mass centroids was obtained by applying the Space Integration Method (SIM). This method has been widely used for the application of tracer techniques to determine longshore transport (e.g., Komar and Inman, 1970; Kraus et al., 1982; Madsen, 1987; Ciavola et al., 1997, 1998). Some variations to the method described by Ciavola et al. (1998) were required to facilitate its applicability to the updrift margin of an inlet.

Coordinates (X_i,Y_i) are assigned to each sampling point, using the topographic data as a basis and linear interpolation and trigonometry to calculate the coordinates in between topographic points. The area represented by each sampling point (A_{Ri}) is then computed as a function of the distance to the surrounding sampling points. Taking into account that not all the cores reached the same sampling depth, and thus there are variations in the distance to the surrounding sampling points, different areas are calculated for each corer for every 0.05 m layer. Once the A_{Ri} is computed, it is possible to calculate the representative volume (V_{Ri}) for each sample,

$$V_{Ri} = A_{Ri}h \tag{1}$$

where h is the height of the samples, $h = 0.05$ m for corer samples and $h = 0.10$ m for semi-surficial samples taken with plastic containers.

The sample volume is then defined as:

$$V_S = \pi r^2 h \tag{2}$$

where r is the radius of the sample (corer or container).

A multiplying factor (F_{mi}), which is used to extrapolate the results of a sample to the entire represented area, is then obtained for each sample by dividing the representative volume (V_{Ri}) by the sample volume (V_S),

$$F_{mi} = V_{Ri}/V_S \tag{3}$$

The mass of FT in each sample (M_{Si}) is calculated as:

(a) For manually counted samples, the number of FT grains in each sample (n) is multiplied by the sand density (ρ_s, 2650 kg/m^3, for quartz sand), and the average grain volume (V_{FT}):

$$M_{Si} = n\rho_s V_{FT} \tag{4}$$

(b) M_{Si} is directly obtained with the FENIX system (Vila-Concejo et al., 2003b).

The mass of remaining FT in each representative area (M_i) is calculated by multiplying the mass of tracer sand found in each sample (M_{Si}) by the multiplying factor (F_{mi}),

$$M_i = M_{Si}F_{mi} \quad (5)$$

The mass of remaining FT for each layer (M_L) is then calculated by summing of all the M_i obtained for each sample within a determined layer,

$$M_L = \sum M_i \quad (6)$$

The total mass of FT remaining in the study area (M_T) is then calculated by summing of all the M_L obtained for each studied layer,

$$M_T = \sum M_L \quad (7)$$

The percentage of remaining FT (PRFT), also called the percentage of recovery (i.e., Madsen, 1987; Ciavola et al., 1997, 1998; White, 1998), can be calculated as,

$$\mathrm{PRFT} = \mathrm{MT} \cdot 100/\mathrm{FT}_{\mathrm{injected}} \quad (8)$$

According to White (1998), the PRFT should be between 60% and 80% for a campaign to be considered successful.

The coordinates of the FT cloud centroid (FT_{CL}) for each layer are then calculated as a weighted average of the coordinates of each sample, using the percentage of M_i ($\%M_i$) represented by each sample with relation to the M_L as the weighting factor.

$$\%M_i = M_i \cdot 100/M_L \quad (9)$$

Therefore, the location of a FT_{CL} is calculated for each studied layer,

$$X(\mathrm{FT_{CL}}) = \sum (X_i \cdot \%M_i)/100 \quad (10)$$

$$Y(\mathrm{FT_{CL}}) = \sum (Y_i \cdot \%M_i)/100 \quad (11)$$

The velocity of displacement of the tracer centroids can be calculated for each layer by dividing the distance (d_L) between the injection point and the FT_{CL}, by the time between the two low tides, in this case 12.5 h (45,000 s). A velocity is then obtained for the FT cloud centroid of each layer,

$$V(\mathrm{FT_{CL}}) = d_L/45,000 \quad (12)$$

The vertical integration of FT_{CL} (FT_C) is then calculated by the weighted average of the coordinates of each FT_{CL}. For this purpose, the percentage of FT present in each layer ($\%M_L$) relative to the total mass of FT found in all the layers (M_T) is used as the weighting factor.

$$\%M_L = M_L \cdot 100/M_T \quad (13)$$

$$X(\mathrm{FT_C}) = \sum (X(\mathrm{FT_{CL}}) \cdot \%M_L)/100 \quad (14)$$

$$Y(\mathrm{FT_C}) = \sum (Y(\mathrm{FT_{CL}}) \cdot \%M_L)/100 \quad (15)$$

The total velocity of the FT_C is then calculated by dividing the distance (d) between the FT injection point and the location of the FT_C by the time between the two considered low tides, (45,000 s),

$$V(\mathrm{FT_C}) = d/45,000 \quad (16)$$

Velocities of displacement were only calculated for the LTS1 of AMI.1, as it is the only experiment that was undertaken on a straight area with unidirectional longshore currents. Experiments undertaken on the swash platform with the combined action of longhsore and bidirectional tidal currents (ebb and flood) provide results not considered to be representative of the trajectory of the FT.

It is necessary to calculate the mixing depth in order to calculate the volume of transported sand. The mixing depth is the thickness of the moving layer where grains of sediment are subjected to vertical and lateral movements by wave action and by the superimposed longshore current (Kraus, 1985). For this study, the mixing depth for each corer sample (Z_{oi}) was calculated according to the methodology proposed by Kraus et al. (1982) and Kraus (1985) as the interval within beach cores where 80% of the FT was found. An average cross-shore profile of sand mixing depth was obtained by calculating the mean mixing depth for the samples located at the same cross-shore position along the beach. The sediment transport rate (Q) is a function of the total velocity ($V(FT_C)$) and the thickness of the active layer (Z_o), that is, the area given by the average cross-shore profile of mixing depth. Therefore, it was only calculated for the LTS1 of AMI.1:

$$Q = V(\mathrm{FT_C}) \cdot Z_o \quad (17)$$

To study the sediment transport patterns at the inlet, four sectors were defined according to the morphology of the study area (Fig. 2). Sector A (P0 to P420) represents the straight part of the updrift beach and transport velocities can be calculated by the approach explained above. Sector B (P430 to P480, up to 100 m from the head of the profiles) represents the upper part of the swash platform located on the easternmost part of Ancão Peninsula that connects the peninsula with the ebb delta. Sector B is naturally separated from the lower part of the swash platform by a tidal channel. Sector C (P430 to P480, seaward of 100 m from the head of the profile) represents the lower part of the swash platform. Sector D (P490 to P650) represents the inner part of the western shore of Ancão Inlet.

4. Results

4.1. AMI.1

4.1.1. Forcing mechanisms

During the afternoon on 20 January waves at the Triaxys buoy consisted of SW swell with T_p of

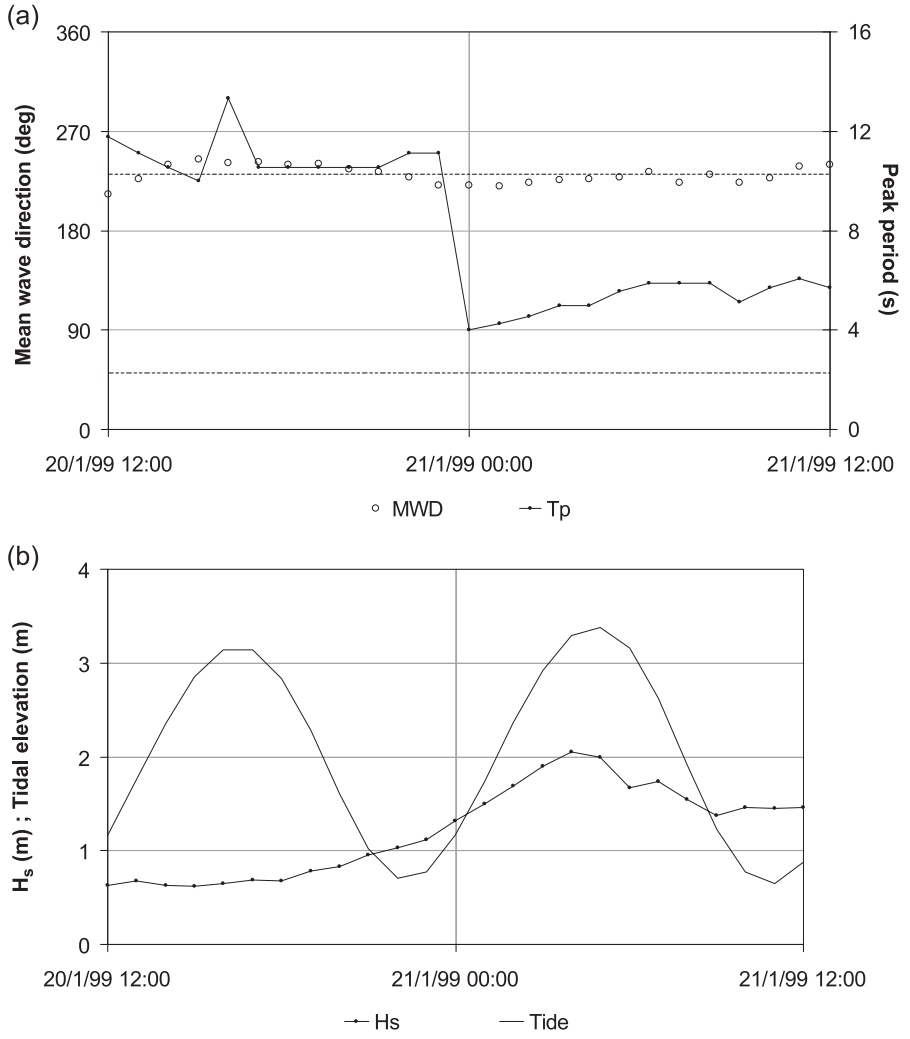

Fig. 3. Forcing mechanisms during AMI.1. (a) Mean wave direction (MWD, deg) and Peak period (T_p, s); (b) Significant wave height (H_s, m) and tidal predictions (m). The dashed lines show the onshore and offshore directions (232° and 52°, respectively).

approximately 12 s (Fig. 3a) and H_s of 0.6–0.7 m (Fig. 3b). Following low tide (23 h), T_p decreased to 5–7 s (Fig. 3a). MWD remained from the SW (Fig. 3a) and H_s increased to 2 m during the high tide, decreasing to values close to 1.5 m for the remainder of the campaign (Fig. 3b). Incident angles were small and while average T_p for AMI.1-1 was twice the value for AMI.1-2, average H_s for AMI.1-1 was half the value for AMI.1-2 (Table 2).

Average speed and direction for EMCMn can be found in Table 2. During the first recorded tide the direction of the resultant currents was between 180°N and 232°N (Fig. 4). Resultant velocities increased towards the end of the recording time reaching maximum values of almost 0.4 m/s. The second tide showed more variability in the resultant current direction with mostly offshore and westwards directed currents at the beginning of the tide. Maximum speeds were less than 0.5 m/s and the average was 0.4 m/s. After the high tide the resultant currents shifted to an eastward direction, reaching speeds of 0.4–0.6 m/s with an average speed close to 0.5 m/s.

4.1.2. Topography

Surf scaling parameter (ϵ) calculations for the beach face showed an intermediate beach whose slope decreases from P0 (tan β_{bf} = 0.09 and ϵ = 4.1) towards the inlet (tan β_{bf} = 0.05 and ϵ = 15 for P400), thus becoming less reflective. Surf similarity parameter (ξ_b) calculated for the beach face showed plunging waves, decreasing its value towards the inlet (from 0.9 for P0 to 0.5 for P400) and, thus, gradually changing to values closer to those of spilling waves. The average slope calculated for the swash platform was 0.006, thus it was very dissipative. These results are related with the existence of the inlet, the inlet channel interrupts the littoral drift producing sand accumulation on the updrift shore of the inlet, thus making the beach more dissipative, and creating the ebb-tidal delta that protects the inlet area from the incident waves.

4.1.3. Tracers

When comparing the natural sand with the painted sand (FT), it can be observed that the mean grain-size decreased and the sorting improved after the painting (Table 3); this is probably due to the sieving process that while taking out the aggregates formed during the painting process, also removed some other elements (such as shells) whose size was very different from the mean grain-size.

Analyses of the samples of AMI.1-1 provided the maps shown in Fig. 5, the eastward sediment transport induced by the nearshore currents (Fig. 4) caused the distribution of the FT to be entirely located on the straight part of the beach (sector A). The percentage of remaining FT (PRFT) during this first sampling was found to be 83%. Most of the FT (90%) was found in the upper layers of the study area (Fig. 5a and b), thus indicating no burial of the tracers. FT contents in the lower layers (Fig. 5d and e) were less than 1% of the PRFT. Average mixing depth was 5.4 cm, reaching maximum values on the beach face (9.6 cm). Most of the transport took place on the beach face of the study area. The computed V(FTc) (vertical integration of the FT velocities found for every layer) was 4.10×10^{-3} m/s, thus indicating eastward sediment transport of about 950 m^3 for that tide (1820 m^3/day). The cloud

Table 2
Average values obtained for the forcing mechanisms measured for each campaign

	Wind speed (m/s)	Wind direction (°N)	H_s (m)	T_p (s)	MWD (°N)	Longshore current velocity (m/s)			Cross-shore current velocity (m/s)			Vertical current velocity (m/s)	
						EMCMn	EMCMo	EMCMr	EMCMn	EMCMo	EMCMr	EMCMn	EMCMo
AMI.1-1	4.4	153	0.8	10.9	233	0.14	–	–	−0.14	–	–	–	–
AMI.1-2	7.0	236	1.6	5.2	227	0.03	–	–	−0.40	–	–	–	–
AMI.2-1	2.3	250	0.4	10.5	268	0.60	0.89	–	0.04	–	–	–	−0.23
AMI.2-2	2.3	210	0.5	5.3	161	0.61	0.70	–	0.05	–	–	–	−0.04
AMI.3-1	1.7	267	0.7	10.9	259	0.40	0.32	0.33	–	0.16	0.33	0.01	–
AMI.3-2	2.7	210	0.6	11.2	256	0.46	0.40	0.26	–	0.17	0.26	0.01	–

Positive signs for currents mean southeastward longshore currents, onshore cross-shore currents and upwards vertical currents. Negative signs imply northwestward longshore currents, offshore cross-shore currents and downwards vertical currents.

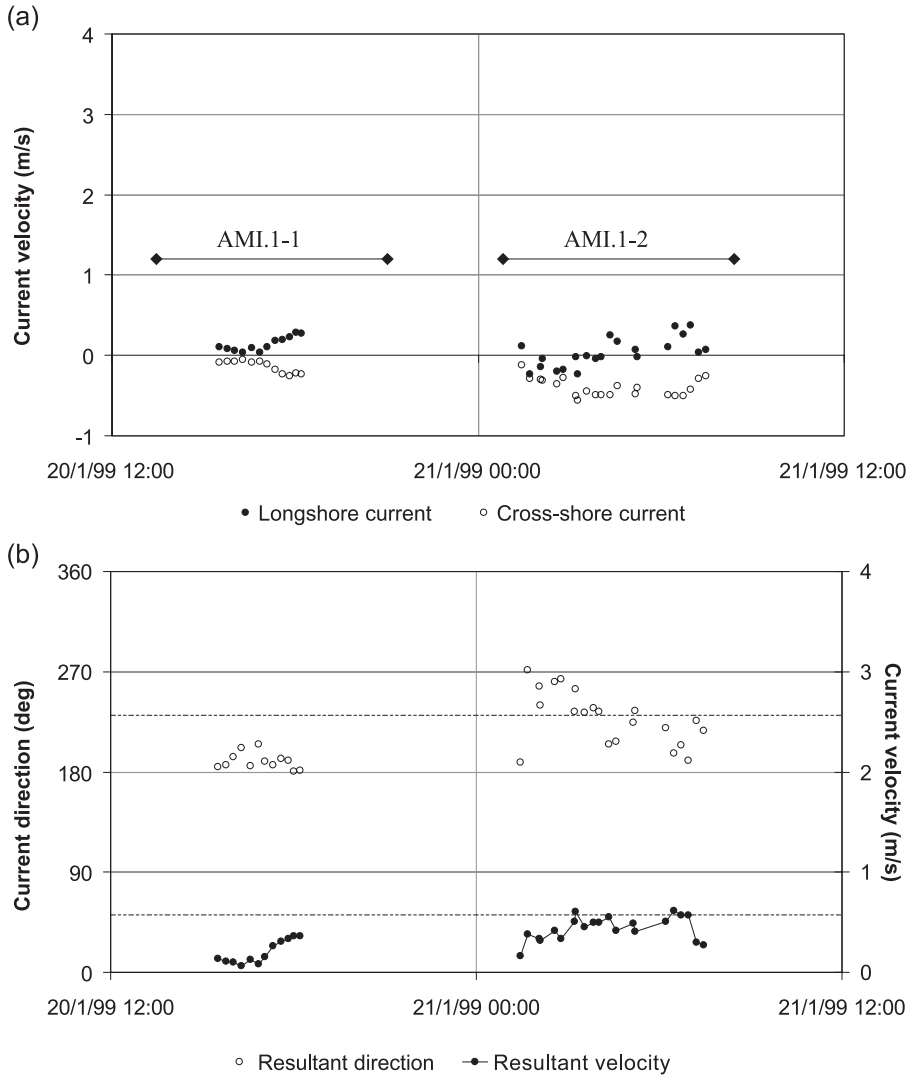

Fig. 4. Currentmeter data from EMCMn during AMI.1: (a) velocity (m/s) of longshore and cross-shore currents (positive values mean southeastward and offshore, negative values mean northwestward and onshore); (b) velocity (m/s) and direction (deg) of the resultant currents. The dashed lines show the onshore and offshore directions (52° and 232°, respectively).

centroid (FTc) was located 177 m from the injection point in a position close to P200, at 60 m from the head of the profile.

Maps obtained for AMI.1-2 sample collection are shown in Fig. 6. PRFT was 67%, meaning that 67% of the injected FT remained after two tidal cycles. Despite the dispersion in the direction of the currents measured for that tidal cycle (see Fig. 4), sediment transport was eastward directed, being transported from sector A towards the inlet (sectors B, C and D). A decrease in FT contents was found from the surface to 15 cm depth (Fig. 6a–c), 55% of the FT was found in these three layers. This was possibly related with the variability in the forcing mechanisms measured at the beginning of the second tide, which induced the burial of the FT. FT content increased for the lower layers (Fig. 6d and e) and the FT distribution patterns for AMI.1-2 at 20 cm depth (Fig. 6d) were very similar to those for AMI.1-1 at 5 cm depth (Fig. 5a). Thus only the

Table 3
Grain-size parameters obtained for the sediment samples taken before (sand) and after (FT) dying with fluorescent paint

Campaign		Mean (mm)	Sorting
AMI.1	Sand	0.47, Medium sand	Moderately well sorted
	FT	0.40, Medium sand	Well sorted
AMI.2	Sand	0.47, Medium sand	Moderately well sorted
	FT	0.55, Coarse sand	Moderately well sorted
AMI.3	Sand	0.82, Coarse sand	Moderately sorted
	FT	1.01, Very coarse sand	Moderately sorted

Note that FT were not sieved for AMI.2 or AMI.3.

upper layers (to 15 cm depth) were analysed. The highest percentage of tracers was observed in sector A (73%), sector C had 16.4% and percentages of 8.5% and 2.1% were found respectively in sectors B and D. FT_{CL} calculated for sector A (Fig. 6a–c) showed higher eastwards transport velocities for the lower layers.

4.2. AMI.2

4.2.1. Forcing mechanisms

Wave direction at the Triaxys buoy was from the W until the morning of 18 February (Fig. 7a). In the afternoon of 18 February, MWD shifted to SE (Fig. 7a). H_s was low (maximum 0.6 m) during the entire campaign (Fig. 7b) and T_p was 10–11 s before noon and decreased in the afternoon. Average H_s, T_p and MWD for periods AMI.2-1 and AMI.2-2 are shown in Table 2.

Measurements from EMCMo and EMCMn showed similar current patterns, the tidal currents were mostly eastward directed (Fig. 8a and b), average current speeds for AMI.2-1 and AMI.2-2 are in Table 2. Vertical currents measured by EMCMo (Fig. 8a) were very weak except during the peak of the eastward tidal current on the first recorded tide when a

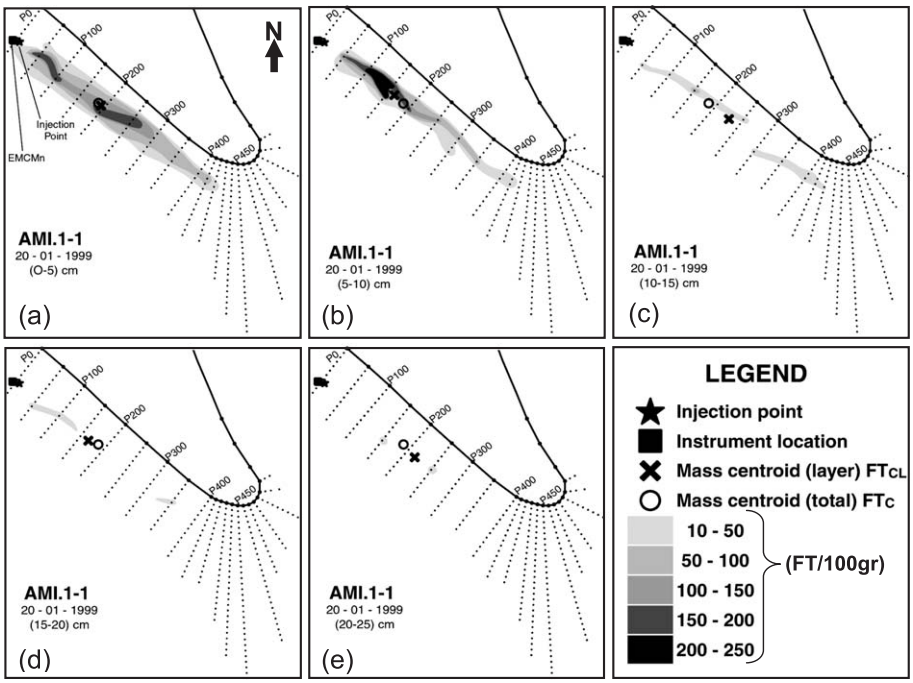

Fig. 5. FT distribution maps for the analysed layers of LTS1 of AMI.1. Locations of the total (FT_C) and partial (FT_{CL}) mass centroids are shown for each layer: (a) 0–5 cm; (b) 5–10 cm; (c) 10–15 cm; (d) 15–20 cm; and (e) 20–25 cm.

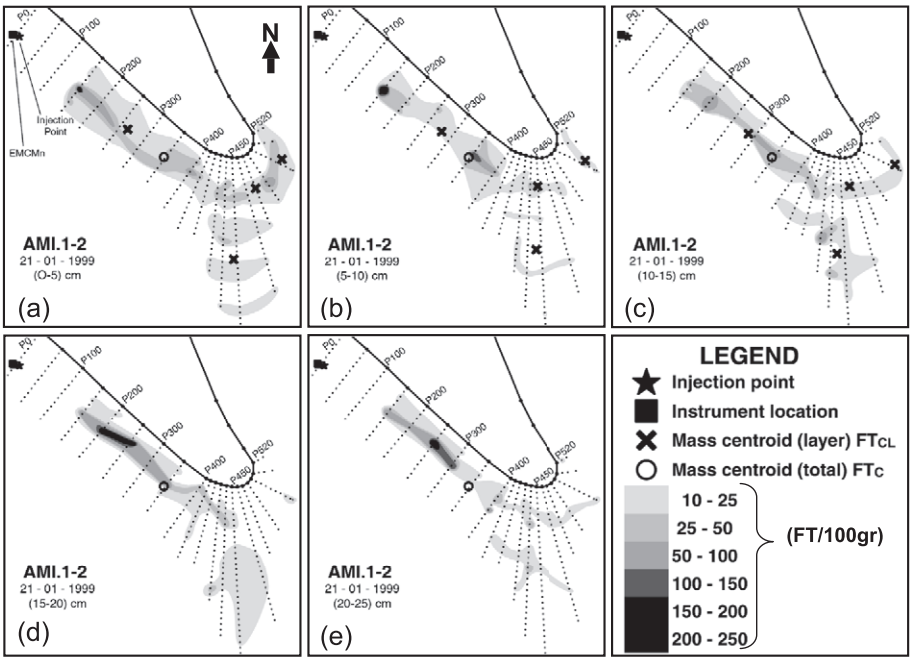

Fig. 6. FT distribution maps for the analysed layers of LTS2 of AMI.1. Locations of the total (FT_C) and partial (FT_{CL}) mass centroids are shown for each layer: (a) 0–5 cm; (b) 5–10 cm; (c) 10–15 cm; (d) 15–20 cm; and (e) 20–25 cm.

downwards directed current with maximum velocity of 0.7 m/s was measured. This is probably related to the existence of large bedforms (megaripples with average wavelengths and heights of about 3 and 0.3 m, respectively) that were observed in the area. Vertical currents during the second tidal cycle were negligible (Fig. 8a). Differences observed between the longshore tidal current velocities measured by EMCMo and EMCMn can also be related to the bedforms mentioned above. Resultant currents calculated for EMCMn are shown in Fig. 8c. Both recorded tides showed similar patterns starting with weak flooding currents (maximum 0.2 m/s). Ebbing currents started 2.5–3 h before the high tide slack having low velocities (maximum 0.2 m/s). Ebb currents increased in speed after the high tide slack and reached 1.5 m/s approximately 1 h after the high tide slack. Current speeds greater than 1 m/s continued for 1.5–2 h before decreasing in speed.

4.2.2. Topography

Topographic profiles measured during AMI.2 were from P400 to P550 since most of the transport occurred on the western shore of Ancão Inlet. Surf scaling and surf similarity parameters on the beach face were only calculated for P400 (representing the part of the study area where influence of bidirectional tidal currents was minimal) providing the following: tan $\beta_{bf} = 0.1$; $\epsilon = 3.6$; and $\xi_b = 0.9$. Therefore, the beach was in an intermediate state (almost reflective) under the influence of plunging waves. Beach face slope was between 0.04 (P430) to 0.19 (P490). The profiles located on the swash platform (P430 and P450) had the least steep slopes due to sediment accumulation. As a consequence of berm development P450 had steeper slopes during AMI.2 than during AMI.1. P470 and P490 also had steep beach faces. However, the shape of these profiles is more controlled by tidal currents than by wave action because of their location in the inlet. The average slope of the swash platform was 0.008 indicating dissipative conditions.

4.2.3. Tracers

Grain-size increased after dying the sand by 0.08 mm that can be considered acceptable for sediment

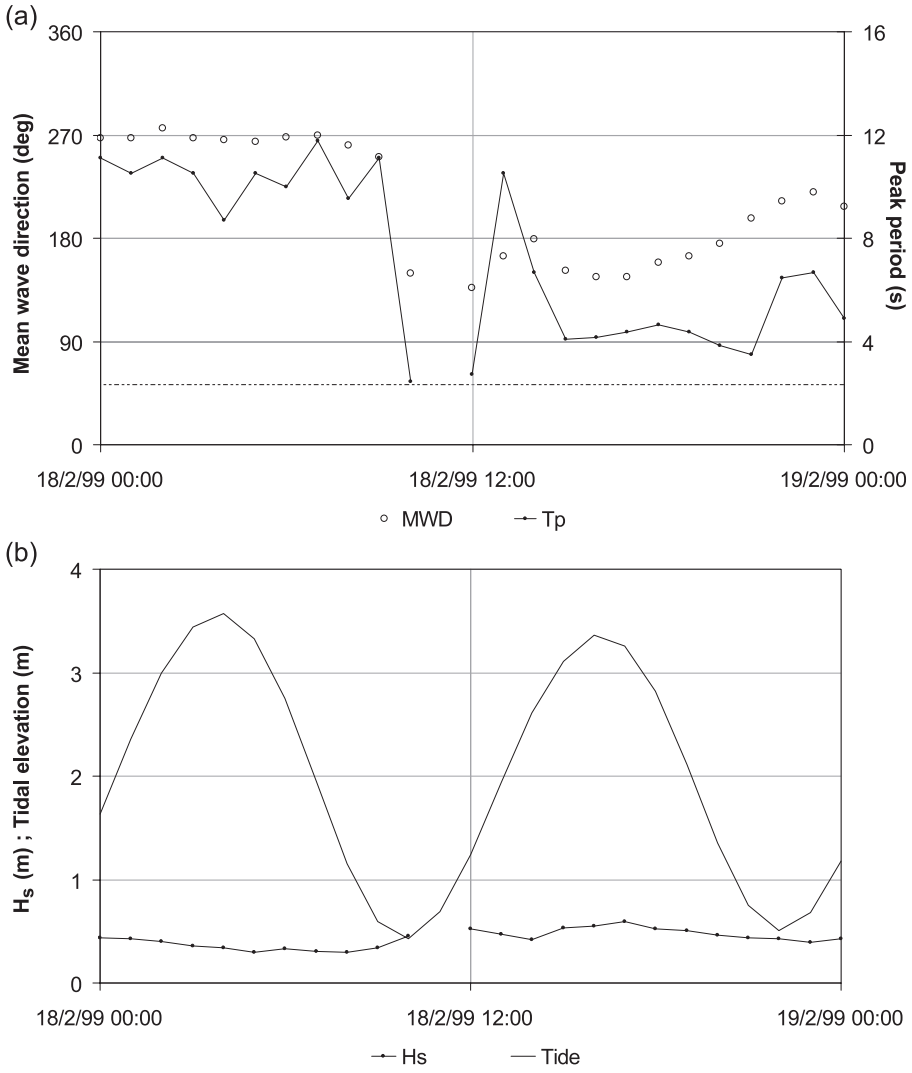

Fig. 7. Forcing mechanisms during AMI.2. (a) Mean wave direction (MWD, deg) and Peak period (T_p, s); (b) Significant wave height (H_s, m) and tidal predictions (m). The dashed lines show the onshore and offshore directions (232° and 52°, respectively).

tracers studies. In this campaign, the sorting of the FT was similar to the sorting of the natural sand (Table 3).

The PRFT obtained for AMI.2-1 (60%) was lower than that obtained for AMI.1. The injection point and both of the EMCMs were located on the southern edge of sector D (Fig. 2). From Fig. 8, it can be seen that the currents acting on the injection point were ebb tidal currents for the majority of time. Resultant ebb tidal currents had a direction of approximately 140°N, implying transport towards the inlet channel. No burial of the FT was detected; however, vertical mixing of the bed sediments was quite high during this campaign. The calculated mixing depth for the swash platform was close to 30 cm, this is probably related with the existence of megaripples. Sectors B and C had 43.8% and 55.8% of the remaining tracers; less than 1% of the FT were found in sector D (Fig. 9a–e). No FT were found in the submarine samples taken in the channel area, however some FT were found in the submarine samples taken in front of the swash platform. The FT_C was located on the northern edge of sector C, on P450.

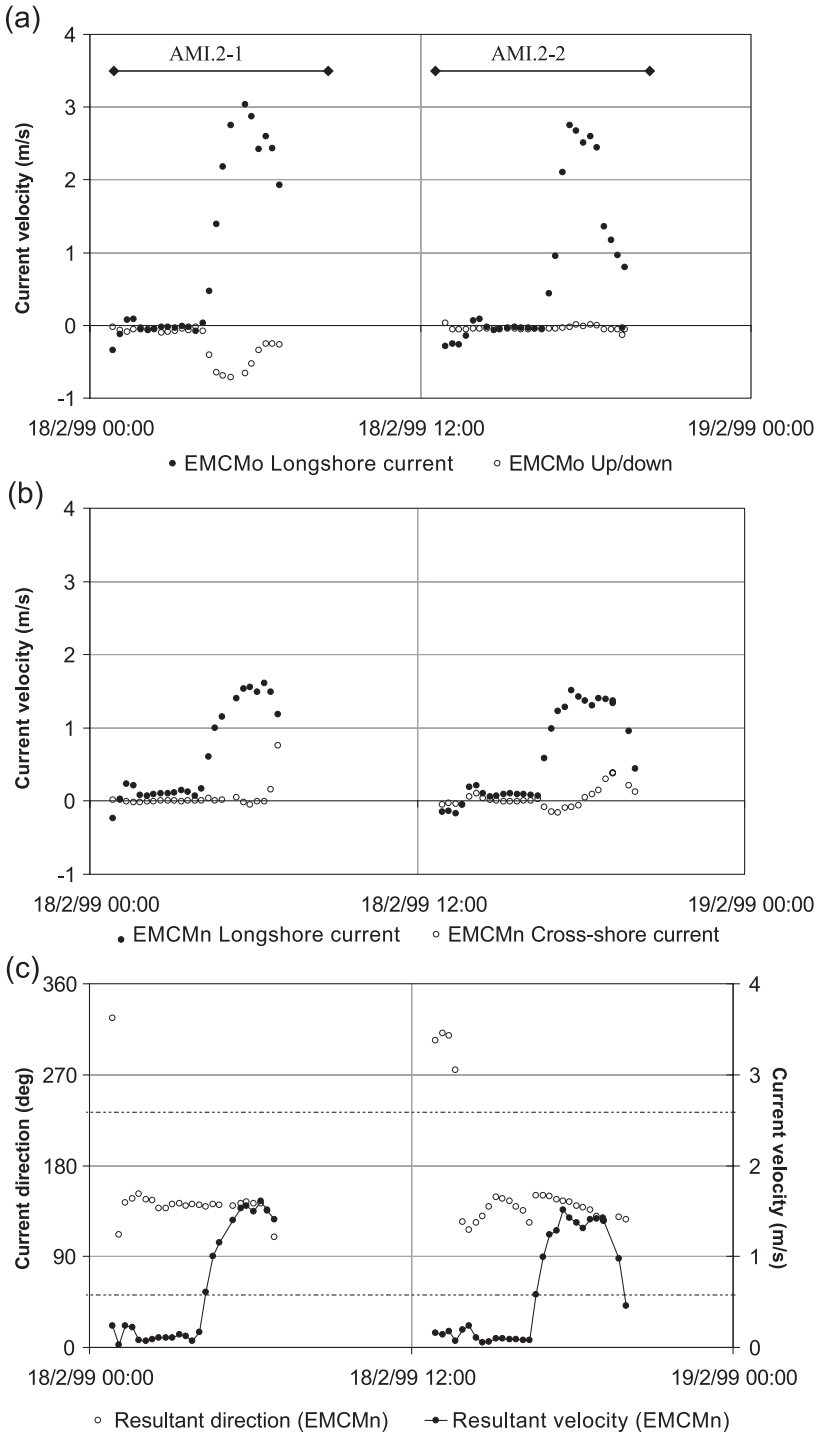

Fig. 8. Currentmeter data from AMI.2: (a) and (b) show respectively EMCMo and EMCMn current velocity data (m/s) (positive values indicate eastward, upward and northward directions, negative values indicate westward, downward and southward directions). (c) Resultant directions (deg) and velocities (m/s) for EMCMn. The dashed lines show the onshore and offshore directions (52° and 232°, respectively).

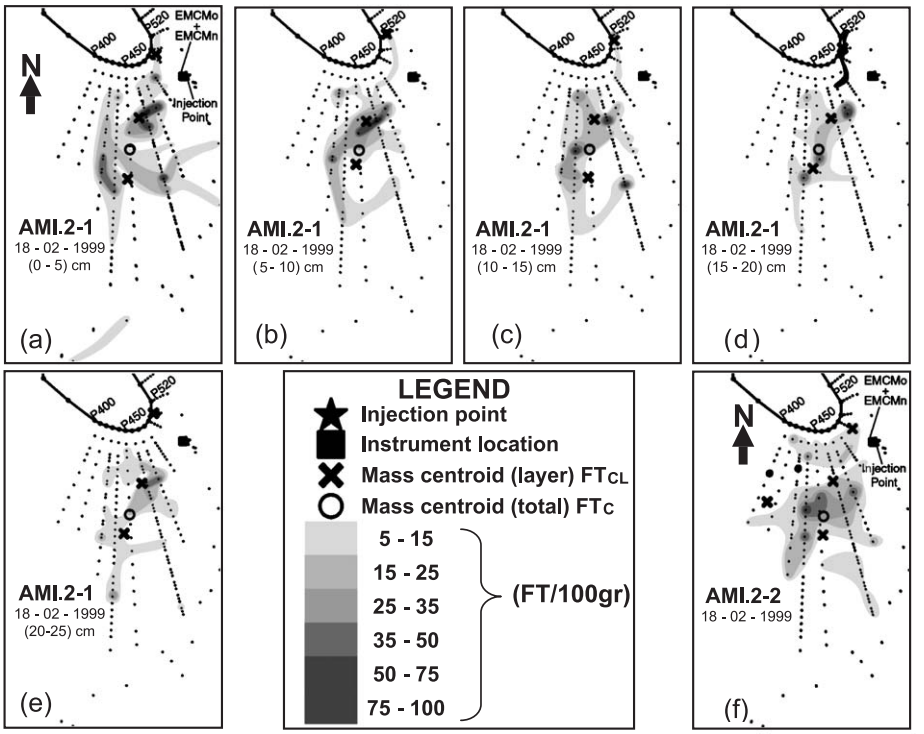

Fig. 9. FT distribution maps for AMI.2. Locations of the total (FT_C) and partial (FT_{CL}) mass centroids are shown for each layer: (a) LTS1 0–5 cm; (b) LTS1 5–10 cm; (c) LTS1 10–15 cm; (d) LTS1 15–20 cm; (e) LTS1 20–25 cm; and (f) LTS2 semi-surficial samples.

The partial FT_{CL} showed small variations with depth but without following any determinable trends.

The distribution map obtained for AMI.2-2 (Fig. 9f) shows high dispersion, only 13% of the injected FT remained in the surface of the study area. The FT_C is almost at the same position as in AMI.2-1 but with a small eastward displacement. Most of the FT were found in sector C (63.9%); sector B had 30.8%; sector A had 4.7%; and sector D had less than 1%.

4.3. AMI.3

4.3.1. Forcing mechanisms

During AMI.3, the offshore MWD was from the W–SW, T_p was 10–12 s (Fig. 10a) and H_s was small ranging between 0.5 and 0.75 m (Fig. 10b). Average offshore H_s, T_p and MWD during AMI.3-1 and AMI.3-2 were very similar (Table 2). The pressure transducer deployed with the RUNTI tripod showed that waves at the inlet had similar T_p to the offshore measurements (Fig. 10a). H_s (RUNTI) was higher on the swash platform than offshore at high tide and lower at low tide (Fig. 10b) because of the natural protection provided by the ebb-tidal delta. At low tide the delta is shallow and the waves break on the delta reducing energy on the inlet shore. In contrast, at high tide the waves propagate across the delta without breaking because of the increased water depth and therefore, reach the inlet shore. Maximum H_s at the inlet approached 1 m during the first recorded tide and decreased slightly during the following tides (Fig. 10b). The average H_s was approximately 0.8 m for both tides (Table 2). It is important to note that because of the flat morphology of the swash platform the incident waves were already spilling by the time they reached the location of measurements. Also, as shown in Fig. 10b, the measured tides at the inlet were similar to the predicted tides. Measured tidal heights were larger than predicted with the maximum difference of approximately 0.2 m occurring at high tide. No direct measurements of MWD were obtained at the

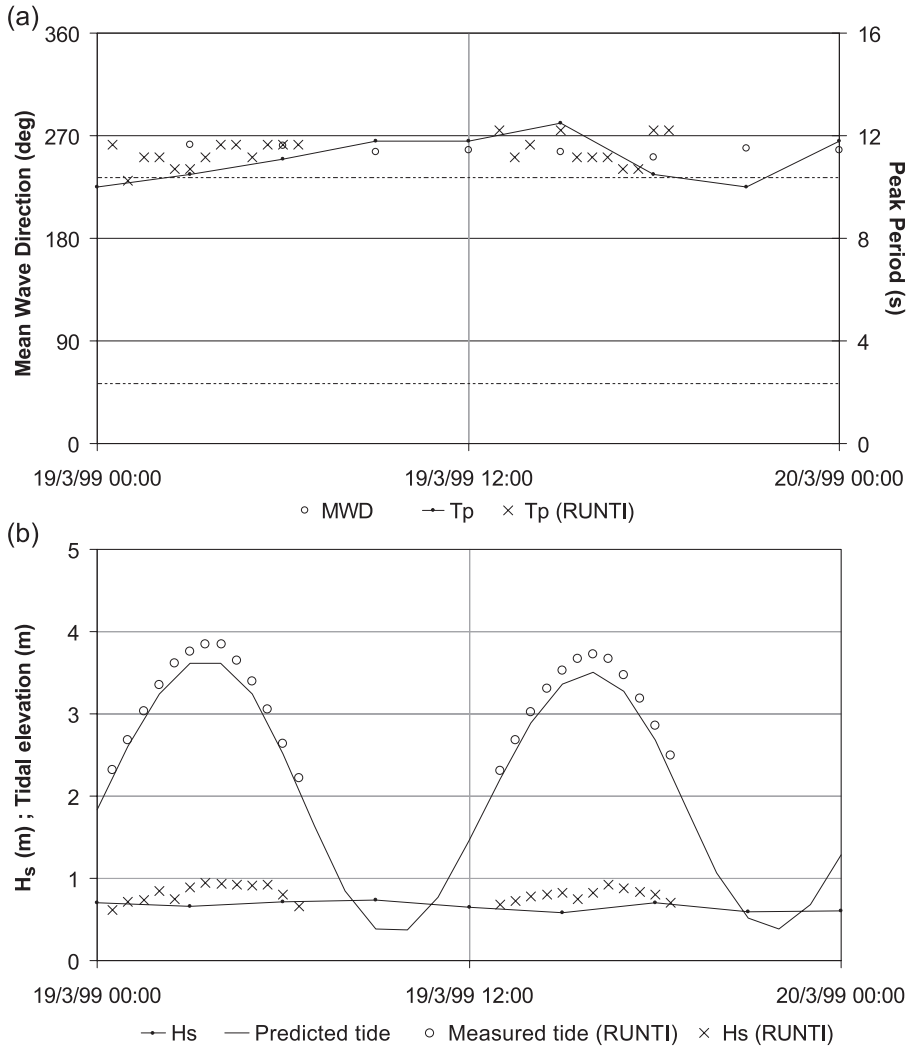

Fig. 10. Forcing mechanisms during AMI.3: (a) mean wave direction (MWD, deg) and Peak period (T_p, s); (b) significant wave height (H_s, m), tidal predictions (m) and RUNTI measured tidal elevations (m). The dashed lines show the onshore and offshore directions (232° and 52°, respectively).

inlet. Visual observations indicated SW waves during the field campaign.

The longshore component of the tidal current showed similar patterns at EMCMo and EMCMn (Fig. 11). The cross-shore component of the tidal current measured by EMCMo (Fig. 11a) was mostly northward directed, and reached a maximum at the same time as the eastward current. The cross-shore current was weaker than the longshore current. Vertical currents were negligible (Fig. 11b). Resultant currents in the internal part of the inlet, computed for EMCMo, showed flooding currents with maximum velocities of 0.4–0.5 m/s (Fig. 11c). Weak ebbing currents with maximum speeds of 0.3–0.4 m/s started approximately 2–2.5 h before the high tide slack. At the high tide slack the resultant currents were very weak (0.1 m/s). Ebbing currents started after the high tide slack. Ebbing currents showed increasing velocities until reaching the maximum velocities (1 m/s) about 1 h after the high tide slack. Current velocities greater than 1 m/s continued for 2–2.5 h before rapidly decreasing in speed.

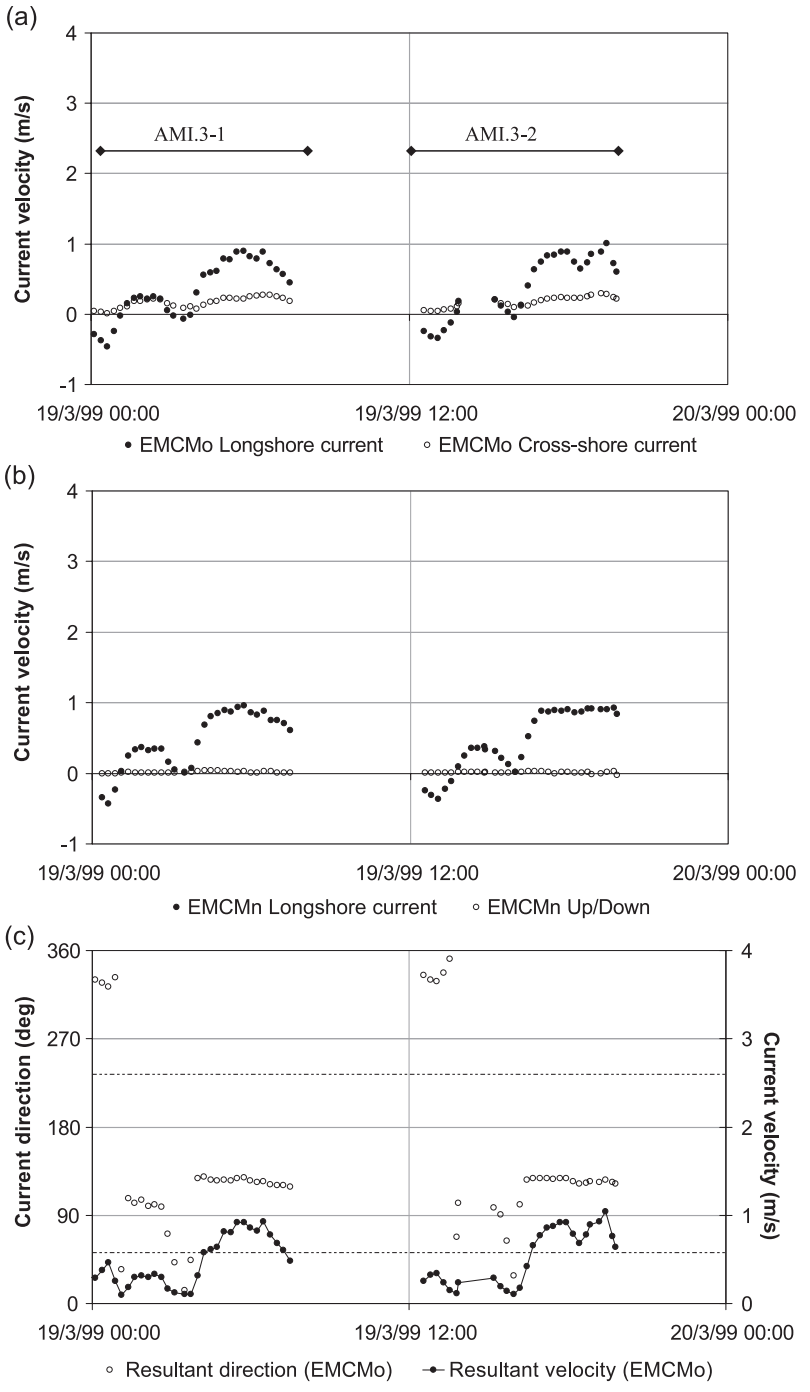

Fig. 11. Currentmeter data measured by EMCMo and EMCMn at the internal part of the inlet channel during AMI.3. (a) and (b) show respectively EMCMo and EMCMn current velocity data (m/s) (positive values indicate eastward, upward and northward directions, negative values indicate westward, downward and southward directions); (c) resultant directions (deg) and velocities (m/s) for EMCMo. The dashed lines show the onshore and offshore directions (52° and 232°, respectively).

Resultant currents on the swash platform (Fig. 12) showed that onshore currents (flooding) reached maximum velocities close to 1 m/s, and lasted until the high tide slack. Offshore currents (ebbing) started after the high tide slack and had weaker velocities (maximum about 0.8 m/s).

Figs. 11c and 12b indicate that each recorded tidal cycle can be separated into three stages: (1) Flooding currents, with higher velocities on the swash platform occur until about 2–2.5 h before the high tide slack. (2) Until the high tide slack flooding currents reach their maximum velocity on the swash platform (1 m/s) and simultaneously weak ebbing currents occur in the inner area (maximum 0.3 m/s). (3) Ebbing currents occur in both areas after the high tide slack, having higher velocities in the internal part. The direction of the ebbing currents on the swash platform (between 270°N and 360°N) indicates westward flow.

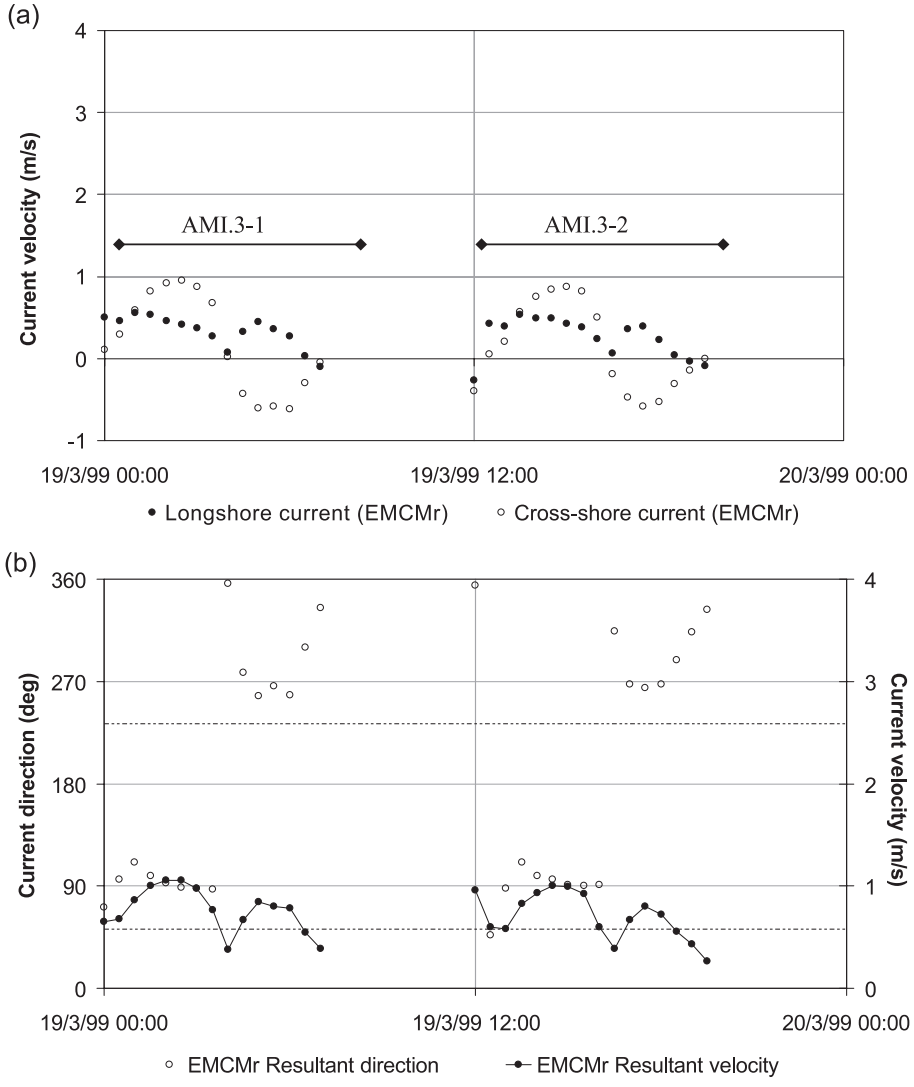

Fig. 12. Currentmeter data measured by EMCMr at the swash platform for AMI.3. (a) EMCMr current velocity data (positive values indicate southeastwards and onshore directions, negative values indicate northwestwards and offshore directions); (b) resultant directions (deg) and velocities (m/s). The dashed lines show the onshore and offshore directions (52° and 232°, respectively).

4.3.2. Topography

Topographic profiles were measured between P350 and P600. Surf scaling and surf similarity parameters for the beach face were only calculated for P400. This profile was chosen because it represents the area where mostly unidirectional currents occur and because it was also measured in the other field campaigns. Values obtained for the parameters are as follows: tan $\beta = 0.1$; $\epsilon = 1.7$; and $\xi_b = 1.4$. Therefore, the beach was subjected to plunging waves and in a reflective state, indicating again some accumulation processes in the beach area close to the inlet. Average slope obtained for the swash platform was 0.011, thus it was in a dissipative state.

4.3.3. Tracers

FT were found to be very coarse implying an increment in the mean size of 0.19 mm and both samples were moderately sorted (Table 3).

The injection point for FT was located in the centre of sector C (see Fig. 2). The computed PRFT for AMI.3-1 was 62%. Most of the FT were found in sector C (89.6%) while sector B had 9.8% and sector D only 0.6%. Some FT were found in the submarine samples collected in front of the swash platform (Fig. 13a). Vertical mixing of the sediments was very high (mixing depth ≈ 25 cm). For all layers there is an area between sectors B and C where no FT were found, this area corresponds to tidal channels. The FT_C was found to be in sector C, about 34 m southwards from the injection point.

The distribution map found for AMI.3-2 (Fig. 13f) shows high dispersion of the FT as well as a very low concentration. Only 1% of the tracers were still remaining in the surface of the study area, 75.4% of them were found in sector C, 13.6% in sector B, 8.6% in sector A and only 2.3% in sector D.

4.4. General morphologic evolution of the swash platform

From AMI.1 to AMI.2 (Fig. 14a), it can be seen that erosion occurred in the inner parts of the inlet (sector D), and that accumulation was observed for the central parts of the swash platform and in the foredune area. Volumetric computations for the total

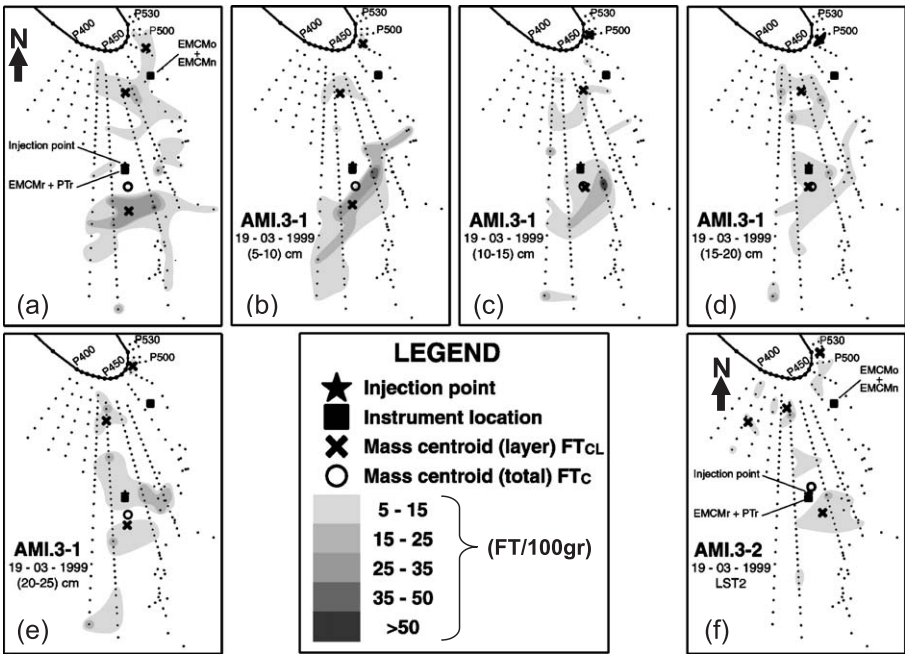

Fig. 13. FT distribution maps for AMI.3. Locations of the total (FT_C) and partial (FT_{CL}) mass centroids are shown for each layer: (a) LTS1 0–5 cm; (b) LTS1 5–10 cm; (c) LTS1 10–15 cm; (d) LTS1 15–20 cm; (e) LTS1 20–25 cm; and (f) LTS2 semi-surficial samples.

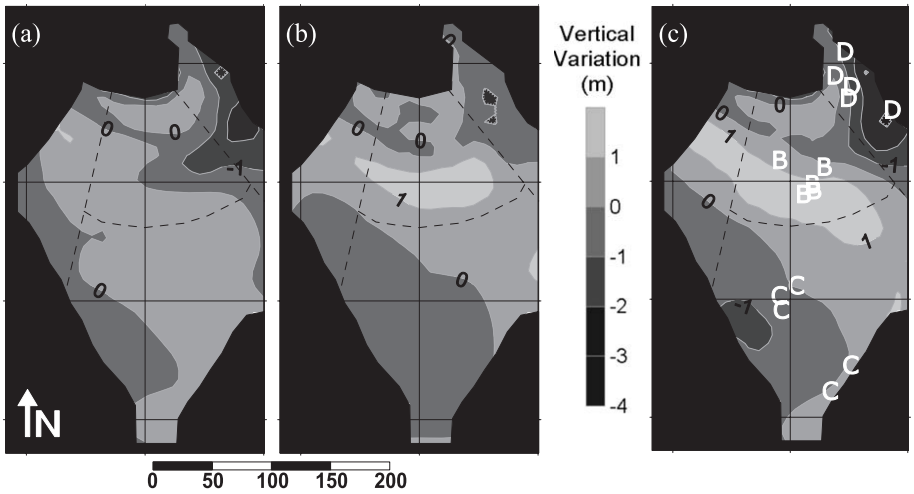

Fig. 14. Isopach maps of the swash platform located on the easternmost part of Ancão Peninsula showing the vertical variations of the morphology (erosion/accumulation): (a) Variation from AMI.1 to AMI.2; (b) variation from AMI.2 to AMI.3; (c) total variation between AM.1 and AMI.3. B, C and D are the total mass centroids obtained for each sector in each campaign.

area indicate a net erosion of 3330 m^3. Between AMI.2 and AMI.3 (Fig. 14b), the erosion occurring in the inner part of the inlet was not as significant as between the first two experiments. Accumulation processes were dominant in the central parts of the sand spit and were more significant than between AMI.1 and AMI.2, especially in the southern part of sector B where over 1 m of accretion was seen. Volumetric computations for the total area indicate a net accumulation of 1880 m^3.

The volumetric evolution of the swash platform located on the western shore of Ancão Inlet (Fig. 14c) indicates a total erosion of -1450 m^3. The accumulation areas, mostly in sector B and the northern part of sector C, show the growth of Ancão Peninsula, with accumulation rates that approach 210 m^3/tide. Erosion rates in sector D were 220 m^3/tide, reaching vertical variations over 3.5 m.

5. Discussion

The work presented here represents an innovative approach to sediment transport studies using tracers in complex environments such as inlet margins. However, there are still some restrictions to the use of FT for a complete and quantitative study of sediment transport at inlet margins. According to Madsen (1987) there are three assumptions in FT theory: (1) advection processes dominate diffusion and dispersion; (2) the natural sand from the beach has similar grain-size properties as the FT; and (3) the transport system must be uniform in the longshore direction. The first assumption can only be accepted for sector A where unidirectional currents largely dominate. The second assumption can be accepted for the three campaigns (see Table 3) since the sand to be painted was extracted from the areas where the injection was to be made. The third assumption can be accepted for sector A, because it is a straight beach and, for the rest of the sectors with some concerns, since they were determined based on the morphology. Therefore, direct quantification of FT transport can only be made for sector A because it is the only sector that fulfils the assumptions given by Madsen (1987). For sectors B, C and D, a semi-quantitative approach based on the definition of sediment transport paths and the transfer between sectors must be established because the three assumptions (Madsen, 1987) are not fulfilled.

5.1. Sediment transport paths

This study and previous studies (i.e., Pilkey et al., 1989; Andrade, 1990; Ciavola et al., 1997, 1998) confirm that the sediment is transported eastward along the updrift beach under SW waves (AMI.1-1,

Fig. 5). Average H_s and T_p during AMI.1-1 was 0.8 m and 8.1 s. The average MWD was approximately 232°N, thus the incident waves were almost shore-normal, resulting in small incident angles that produced the longshore currents. During AMI.1-1, the sediment transport computed using the tracer data (see Section 4.1.3) was 1820 m^3/day (950 m^3/tide). Balouin et al. (2001), using a smaller amount of tracers, studied the sediment transport at a swash bar on the same swash platform where this study was performed. The results of Balouin et al. (2001) showed a sediment transport of approximately 370 m^3/day (190 m^3/tide) for 28 February 1999. Offshore waves for that day were from the SW with H_s ranging from 0.8 to 1.1 m and T_p approximately 11 s. Ciavola et al. (1997) calculated transport rates between 200 and 1200 m^3/day under short period SW waves with average H_s ranging from 0.28 to 0.44 m from tracer studies performed at Culatra Island (Fig. 1). According to Costa (1994), mean winter H_s and T_p at the study area are 1.15 m and 9.5 s, respectively, and waves approach from W–SW approximately 64% of the time during winter. Therefore, the SW waves measured during this study and those measured by Balouin et al. (2001) and Ciavola et al. (1997) are within the expected ranges for SW winter waves in the study area but slightly inferior to the average values. Thus, it can be said that daily gross littoral drift in the area, for SW winter-calm conditions, ranges from 200 to 1820 m^3/day.

The general morphologic evolution of the swash platform (see Section 4.4) showed that sediment accumulation on the swash platform (mostly sector B) was 210 m^3/tide. Accumulation rates found in this area are in agreement with those obtained by Balouin et al. (2001) for the same area but using different methodology (190 m^3/tide). Therefore, accumulation in sector B represents about 20% of the gross littoral drift calculated for AMI.1 (950 m^3/tide).

Sediment transported to the inlet is subjected to tidal currents. Tracer results from AMI.1-2 (Fig. 6) showed that after the second tidal cycle, 73% of the remaining tracers were located in sector A and 27% entered the area of the swash platform. It should be noted here that the percentage of sediment remaining in sector A could have been lower if westward directed currents did not occur during the first stages of AMI.1-2 (see Fig. 4). Of the FT that entered the swash platform, 31.5% was found in sector B, 60.7% in sector C and 7.8% in sector D. According to the currents measured during this campaign (Fig. 4) and to the FT distribution maps (Fig. 6), it seems reasonable to establish direct sediment transport from sector A to sectors B and C. However, data from this campaign does not allow the establishment of the sediment transport paths to sector D.

Currentmeter data from AMI.2 and AMI.3 can be used to determine the current patterns on the inner inlet margin (sector D) and swash platform (sector C). According to the currentmeter data from AMI.2 and AMI.3 (see Sections 4.2.1 and 4.3.1), three tidal stages (TS1, TS2 and TS3) can be defined inside each tidal cycle. TS1 occurs until 2–2.5 h before the high tide slack, and during this stage flooding currents occur in both sectors, being stronger in sector C. TS2 lasts until the high tide slack, and during this stage flooding currents reach their maximum velocity on the swash platform (sector C, see Figs. 11c and 12b) while weak ebbing currents occur in sector D (see Figs. 8c, 11c and 12b), indicating the existence of an anticlockwise current gyre located over sector D. During TS3, which occurs after the high tide slack, ebbing currents occur in both sectors, being stronger in sector D (see Figs. 8c, 11c and 12b), currents measured in sector C were directed westwards (Fig. 12b) that together with the SW incident waves (Fig. 10a) suggests the existence of a clockwise current gyre.

Sediment transport paths on the swash platform became clearer with the FT results obtained for AMI.2 and AMI.3 (see Figs. 9 and 13). For both campaigns, almost no tracers were found close to the injection point, reflecting the highly dynamic nature of the system, and the value of PRFT was close to 60% for the LTS1 of each campaign, which according to White (1998) is inside the range of values considered as 'good'. FT distribution was similar in both campaigns with the maximum FT concentration in sector C, followed by sector B, and sector D where almost no FT were found. Simultaneously, some FT were found in the eastern part of sector A and in the submarine samples taken in front of the swash platform.

Combining currentmeter and FT data from AMI.2 and AMI.3 the following sediment transport paths are established:

(1) During TS1, the sediments are transported from sectors C and D towards the inner parts of the

inlet system. Once the water floods sector B, the sediments in this sector are also transported towards sector D.

(2) During TS2, while flooding currents are still acting in sectors B and C, an anticlockwise circulation gyre, internal gyre (IG), is established in sector D producing offshore directed currents in that sector (Fig. 15a). Therefore, while sediments from sectors B and C are transported to the inner parts of the inlet (including sector D), sediments from sector D are partially re-circulated due to the influence of the IG. The IG was observed during the fieldwork campaigns, and described by Williams et al. (2003), but its existence has been confirmed by the analyses of current data during AMI.3. The development of the IG (Fig. 15a) is possibly related with the morphology of the area and the intensity of the flow: while the flood delta is still emerged the flooding currents are constricted to the internal channel located at the back of Ancão Peninsula, once the flood tidal delta is under water the flooding currents which are now more spread interact with the delta and develop an anticlockwise gyre.

(3) During TS3 ebbing currents affect all of the swash platform (towards the ebb jet in the inlet channel for sector D and westward directed for sector C), thus the possible explanation for the presence of tracers in sectors A, B and C is the development of a clockwise circulation gyre, external gyre (EG) in the external part of the inlet (Fig. 15b). Ebbing currents in sector D are very strong producing sediment removal and consequent erosion, which is in agreement with the results from the morphologic evolution of the swash platform (see Section 4.4). The existence of an external gyre (EG) on the updrift margin of a tidal inlet has been reported by several authors for inlets in different parts of the world (i.e., Oertel, 1972; Smith and FitzGerald, 1994; Dyer and Huntley, 1999; FitzGerald et al., 2000) and also in previous studies of Ancão Inlet (Williams et al., 2003). According to several authors (i.e., Oertel, 1972; Smith and FitzGerald, 1994), EG development (Fig. 15b) results from wave–current interaction at the terminal lobe of the ebb delta. According to the FT distribution patterns for AMI.2 and AMI.3 (Figs. 9 and 13, respectively), the current velocities in the gyre are high enough to permit sediment re-circulation during a single tidal cycle (e.g., FT found in the eastern part of sector A for AMI.2 and AMI.3). The EG explains the high concentration of FT found in sectors B and C for all the campaigns, and the sediment transport towards sectors A, B and C for AMI.2 and AMI.3. The EG also contributes to the explanation of the sediment accumulation found on the central areas of the swash platform that was observed in the

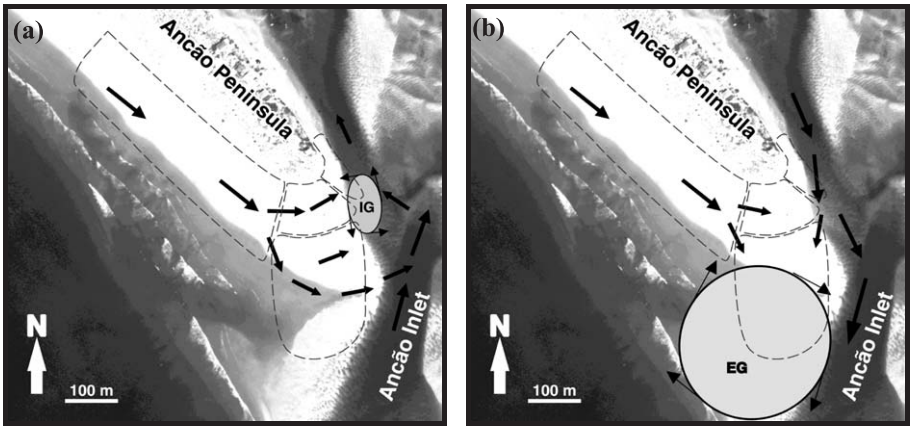

Fig. 15. Conceptual model for sediment transport paths at the updrift margin of an inlet: (a) flooding conditions and (b) ebbing conditions. Dashed lines show the division between the considered sectors; arrows show the sediment transport pathways; IG is the internal gyre; and EG is the external gyre.

medium-term volumetric and morphologic analysis (Fig. 14).

It is important to note that the sediment transport paths found for the swash platform updrift of Ancão Inlet were very similar for the three campaigns. Location of FTc for sectors B, C and D (Fig. 14c) was very similar for all the campaigns, the standard deviation of the coordinates was calculated providing mean values of 11.8, 32.0 and 17.1 m, respectively. FTc for sector B shows the lowest variations in its position, in Fig. 14c it can be seen that the location of FTc for this sector is coincident with the areas where accumulation processes related with the growth of Ancão Peninsula were occurring. Therefore, under SW winter calm conditions, the sediment transport paths seem to be dependent on the tidal conditions (that were very similar during all campaigns) and quasi-independent of the waves and wind conditions (which showed some variations in between campaigns). However, it seems reasonable that the sediment transport magnitudes under SW winter calm conditions will be greatly influenced by changes in the incident waves, or under the influence of very strong wind, even if there are no variations in the sediment transport paths. Sediment transport paths are expected to be very different under SE or storm (both from SW and SE) conditions.

A schematic design for the sediment transport paths defined for Ancão Inlet is shown in Fig. 15. Tidal flooding just before the high tide slack is shown in Fig. 15a where the IG can be observed. The paths are directed towards the internal areas of the inlet, and the transport occurs from sector A to sectors B and C, and from sector B to sector D where part of the transported sediment can be temporarily trapped by the IG; sediment transported from sector C goes directly to the inlet channel and as it travels towards the internal areas, it can also be partially trapped by the IG. Sediment transport paths for tidal ebbing are shown in Fig. 15b, along with the approximate location of the EG. Under the influence of the incident waves and winds downdrift transport occurs in sector A towards sectors B and C. Simultaneously, strong ebb tidal currents flush the sediments from the internal areas of the inlet towards the ebb jet that reaches the ebb delta. Some of the sediments transported by the ebb jet are trapped by the EG and re-circulation towards the easternmost part of sector A and sectors B and C occurs.

5.2. A semi-quantitative conceptual model for sediment transport on the swash platform

With the results obtained for the three campaigns, a semi-quantitative conceptual model can be defined for the sediment transport on the swash platform located on the western shore of Ancão Inlet under SW conditions. However, an analysis of the sediment losses that occurred during the campaigns is needed. Results from the calculation of sediment loss were found to be very similar for both of the studied tides for AMI.1 (17% and 16% for AMI.1-1 and AMI.1-2, respectively) and for AMI.2 (40% and 47% for AMI.2-1 and AMI.2-2, respectively). However, the two tides studied showed very different percentages of sediment loss for AMI.3 (38% and 61% for AMI.3-1 and AMI.3-2, respectively). Hydrodynamic conditions during the two tides of AMI.3 were very similar, thus the explanation of this difference is probably related with the nature of the sample collection. Vertical mixing of the sediments on the swash platform was very high (see Section 4.3.3) and AMI.3-2 was performed collecting semi-surficial samples with plastic containers. Therefore it could be possible that the FT were completely mixed with the natural sediments or that they were buried during accumulation processes on the platform. As a consequence, the tracers results obtained through corer samplings (both LTSs for AMI.1 and the LTS1 for AMI.2 and AMI.3) are considered to be more reliable and are the ones used for the semi-quantitative conceptual model.

The proposed model is based on the forcing mechanism conditions and results obtained for the AMI campaigns, therefore, the following restrictions are to be taken into account in its application: (a) Incident waves are from the SW, with average values for H_s ranging from 0.4 to 1.6 m and for T_p from 5.2 to 11.2 s, thus according to Costa (1994) correspond to typical calm to moderate SW conditions for the study area, therefore, tide-dominated processes are assumed; (b) Sediment losses found for the tracers are assumed to be real losses of sediment (i.e., sediment is transported outside the study area) and not the result of under sampling (results from AMI.2-2 and AMI.3-2 are not used for the model).

The model has two stages that occur between consecutive low tides (beginning of first tide, time 0, $t=0$; end of first tide and beginning of the second one, time 1, $t=1$; and, end of the second tide, time 2, $t=2$) and includes the effect of both the external and the internal gyres determined within this study. Stage 1 occurs between $t=0$ and $t=1$ and represents the sediment arrival to the swash platform from the updrift beach. The distribution and loss of sediments inside sectors B, C and D occurs according to the results obtained from the FT analyses for AMI.1-2, such that the sediment injection occurs from sector A. Stage 2 occurs between $t=1$ and $t=2$ and represents the reworking of the sediments inside the swash platform. Results from AMI.2-1 and AMI.3-1 are used to determine the distribution and the losses of sediment, therefore the reworking of the sediments occurs from sectors D and C, respectively. The steps of the model are explained in the following paragraphs and a schematic of the model is shown in Fig. 16.

5.2.1. Stage 1

At time $t=0$ (low tide), a certain amount of sediment (M_A) arrives at the western limit of the swash platform (the limit between sectors A and B). According to results obtained for AMI.1-2, after one tidal cycle ($t=1$, low tide), the loss of sediments (L_1) is 17% of M_A. Therefore the percentage of remaining FT at $t=1$ ($PRFT_1$) can be calculated as

$$PRFT_1 = M_A - L_1 \tag{18}$$

$$PRFT_1 = 0.83M_A \tag{19}$$

This sediment is transported onto the swash platform following the sediment transport paths of Fig. 15, the following distribution of FT is found: sector B has 31% ($SB_1 = 0.31 \cdot PRFT_1$), sector C has 61% ($SC_1 = 0.61 \cdot PRFT_1$) and 8% of the FT are in sector D ($SD_1 = 0.08 \cdot PRFT_1$).

5.2.2. Stage 2

Stage 2 of the model assumes that the sediment injection is in sector D (to follow AMI.2-1 patterns) and in sector C (to follow AMI.3-1 patterns). Therefore the assumption is needed that the sediments remaining in sector B (SB_1) are directly transported towards sector D and are reworked from there (Fig. 15). Simultaneously, the volumetric evolution of the swash platform showed that sector B acts as a sediment sink and traps approximately 20% of the gross littoral drift (see Section 4.4). Therefore, for stage 2 it is assumed that there are two masses of sediment to be reworked: one from sector D (M_{2D}) is formed by the addition of SD_1 plus the 80% of SB_1, and the other from sector C (M_{2C}) corresponds to SC_1:

$$M_{2D} = SD_1 + (0.80 \cdot SB_1) - L_{2D} \tag{20}$$

$$M_{2C} = SC_1 - L_{2C} \tag{21}$$

where L_{2C} corresponds to the losses determined for sediment reworking from sector C for AMI.3-1 ($L_{2C} = 0.38 \cdot SC_1$) and L_{2D} corresponds to the losses determined for sediment reworking from sector D for AMI.2-1 ($L_{2D} = 0.40(SD_1 + 0.80 \cdot SB_1)$).

The quantification of the percentage of remaining tracers at time $t=2$ is made as follows:

$$PRFT_2 = PRFT_1 - L_2 \tag{22}$$

where the loss of sediment at $t=2$ is defined as:

$$L_2 = L_{2C} + L_{2D} \tag{23}$$

According to AMI.2-1 the distribution of the sediments reworked from sector D (M_{2D}) is approximately 44% in sector B, 56% in sector C and 0.3% remains in sector D. According to AMI.3-1, the distribution of the sediments reworked from sector C (M_{2C}) is 90% remaining in sector C, 10% in sector B, and 1% in sector D. Thus, the total distribution of the sediments in the system is as follows:

$$SB_2 = 0.20SB_1 + (0.44M_{2D} + 0.10M_{2C}) \tag{24}$$

$$SC_2 = 0.56M_{2D} + 0.90M_{2C} \tag{25}$$

$$SD_2 = 0.003M_{2D} + 0.01M_{2C} \tag{26}$$

According to the model and assuming a sediment injection in sector A of $M_A = 1000$ kg for $t=0$: after one tide (at $t=1$) 830 kg of sediment would still remain in the system, of which 257 kg would be in sector B, 506 kg would be in sector C and only 66 kg would be in sector D. After two tides ($t=2$), 529 kg of the sediments injected at $t=0$ would remain in the

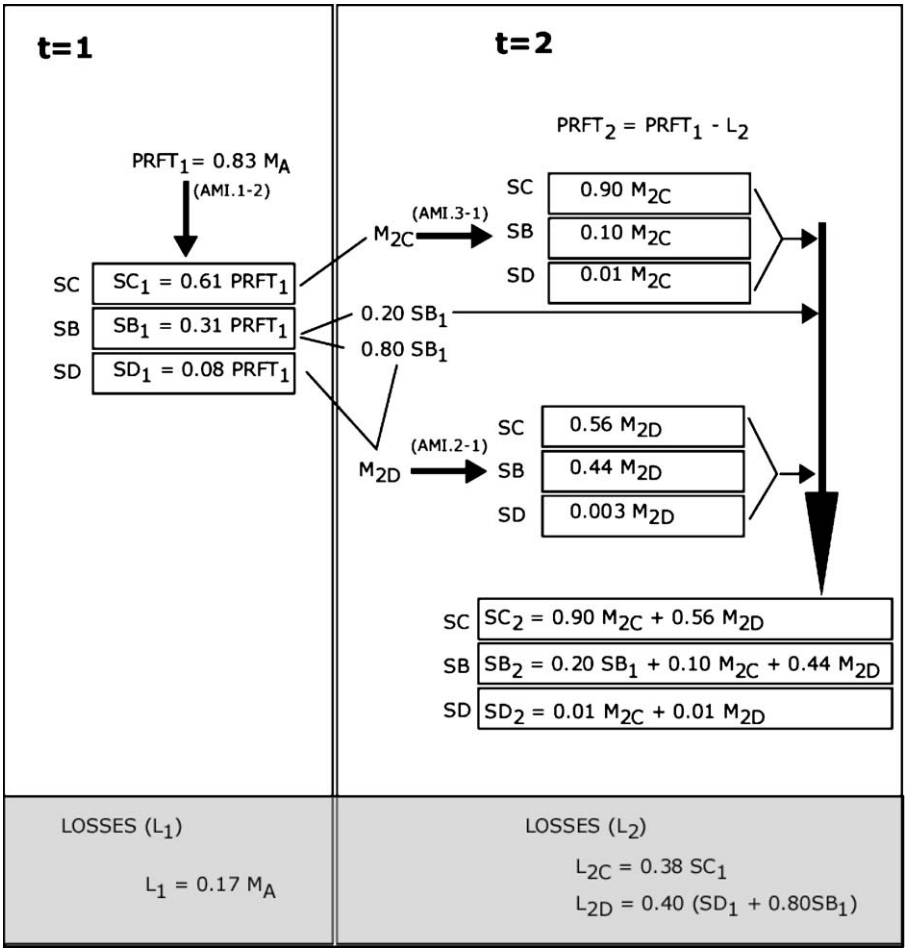

Fig. 16. Schematic of the semi-quantitative conceptual model.

system. Distribution at $t=2$ would be as follows: 155 kg in sector B, 374 kg in sector C, and 4 kg would be in sector D. Therefore, after two tides only 53% of M_A would remain in the swash platform system and, thus, the sediment loss would be 47% of M_A. However, due to the new inputs of sediment into the system every tide through the littoral drift, it is important to note that sediment loss in this case, does not correspond to erosive processes. Assuming a constant input of 1000 kg/tide, after two tides, the sediments to be reworked at the swash platform would be 1359 kg (529 kg remaining from $t=0$, plus 830 kg remaining from a new input occurring at $t=1$). It is important to note that due to the EG some of the sediments would be found in sector A; however, the presented model only takes into account the sediment transport processes on the swash platform.

Loss of sediments can be due to several factors, i.e., accumulation on the ebb/flood delta, inner channels, sediment by-pass or offshore expulsion through the ebb jet. According to Williams et al. (2003) and Morris et al. (2004) during the time of the fieldwork campaigns Ancão Inlet was in a transitional state (called MOR3), recovering after post-storm conditions (a large SW storm occurred in December 1998). According to Williams et al. (2003) during the MOR3 state, tidal flows are strong causing the erosion of the flood delta which supplies sediment that is transported offshore to feed the ebb delta and that together with the littoral drift makes

possible the restoration of the beach and spits. The existence of an EG in a tidal inlet system has been proposed by several authors; however, the full extent of such a gyre is known to be variable (Oertel, 1972). The EG in the Ancão Inlet system cannot be quantified with the data in this study. However, Vila-Concejo et al. (2003a) found that the ebb delta was the only morphologic unit of the inlet that showed continuous accumulation during the first 2 years of the evolution of Ancão Inlet. Therefore, it seems likely that sediment losses from the swash platform were transported offshore by the strong tidal flows to feed the ebb delta and that some of them were re-circulated by the EG to restore the updrift beach (Fig. 15b).

5.3. Applicability

Tidal inlets have been widely studied; however, according to the literature, most of the studies have been performed at inlets in the US Atlantic coast or for the Dutch and German Friesian Islands. This contribution represents a detailed study, using an innovative approach, of the sediment transport patterns of an inlet that is located in a relatively unstudied area in terms of short-term processes. Circulation patterns are specific to each inlet but certain processes like ebb or flood dominance, preferred channels on ebb and flood tide and gyre formation and migration amongst others, are common to many inlets (Militello and Hughes, 2000). The short-term sediment transport patterns found for Ancão Inlet are in agreement with other long-term studies performed in the same area (i.e., Morris et al., 2004; Vila-Concejo et al., 2003a; Williams et al., 2003). Also, they agree with the general transport patterns that were found in other inlet studies (i.e., Oertel, 1972; Smith and FitzGerald, 1994).

The semi-quantitative conceptual model presented here assumes oceanographic and climatologic conditions similar to those measured during the AMI campaigns. It has been developed as a tool to understand what happens to the sediments that arrive at the swash platform from the updrift beach under SW conditions. Therefore other sediment sources, such as the tidal deltas or the inner channels, are beyond the scope of this study and were not taken into account, but could be important. Other sediment transport studies in the area including both deltas and the downdrift beach would be needed to fully understand the sediment transport patterns in the entire inlet system as well as the sediment bypassing mechanisms. The semi-quantitative conceptual model herein presented is not a sediment budget in the sense that it does not include all the inputs and outputs of sediments. It rather represents, in a semi-quantitative way, the transport paths followed by the sediments that, under certain conditions, are supplied to the updrift margin of an inlet by one of the main sediment sources: the littoral drift. These results, together with the results of other campaigns covering all of the inlet area, could be used to validate numerical models such as 3D-INLET (O'Connor et al., 2000) that simulate waves, currents, sediment and morphology.

The use of tracers for the study of sediment transport patterns at tidal inlets is an efficient and relatively low-cost technique that can provide accurate results. It is expected that, under similar conditions, the magnitude of the sediment transport patterns at other inlets with analogous characteristics (i.e., size, tidal prism, incident waves, grain-size) will be comparable to those obtained for Ancão Inlet with the semi-quantitative conceptual model.

6. Conclusions

In recent years, the study of the sediment transport pathways and magnitudes has proved to be a difficult obstacle for the definition of a sediment budget in inlet areas. The division of the study area into morphologically defined sectors was a key step in the successful application of the SIM methodology to such a complex area. Also, the fact of working with a geo-referenced coordinate system instead of the traditionally used distances to the injection point increased the reliability and accuracy of the method. Sediment transport pathways were defined; however, sediment transport magnitudes could only be computed for the straight sector of the study area. Gross littoral drift for the study area was 950 m^3/tide, during calm-moderate winter SW conditions.

The combination of the tracer analyses, forcing mechanisms and topographic evolution of the study area permitted the definition of sediment transport

pathways. Three tidal stages were differentiated for every tidal cycle (TS1, TS2 and TS3). TS1 occurs from the low tide slack until 2–2.5 h before the high tide slack, during this time, flooding currents are registered in all of the inlet area. During this stage, transport towards the inlet and its inner areas occurs. TS2 occurs after TS1 and implies strong flooding currents occurring on the swash platform while an anticlockwise gyre (internal gyre, IG) develops as a consequence of the interaction of the flood delta with the flooding currents. During TS2 sediment transport on the swash platform is directed towards the inlet; however, in the inner parts of the inlet ebbing transport can occur due to the re-circulation of the sediments inside the IG. TS3 occurs after the high tide slack and ebbing currents are registered both on the swash platform and in the inner sectors of the inlet. Transport on the swash platform was found to be westwards thus, together with the SW incident waves, implying the existence of a clockwise external gyre (EG). Sediment transport during this tidal stage is offshore directed in the inner parts of the inlet under strong ebbing currents and westwards directed on the swash platform implying re-circulation of the sediments towards the west and upper parts of the swash platform.

To quantify the sediment transport at the updrift margin of the inlet, the integrated results were used to develop a semi-quantitative conceptual model. The model was developed to quantitatively describe the sediment transport pathways and magnitudes followed by a known mass of sediment arriving at the swash platform. Application of the model is restricted to SW winter calm conditions and assumes that the sediment losses are the result of the sediment going out of the system and are not the result of under sampling during the tracer experiments. According to the model, most of the accumulation of sediment occurs on the swash platform, which is consistent with the way an inlet migrates or a spit grows, while the inner sectors of the inlet margin are eroding and thus, do not retain the sediment that arrives there. After one tidal cycle 83% of the initial mass of sediment remains on the swash platform. The reworking of the same mass of sediments during the following tidal cycle results in 53% of the initial mass of sediments remaining in the system after two tidal cycles.

More sediment transport studies, including studies on the scale of the entire inlet, at this and other inlets are needed to fully understand sediment transport pathways and magnitudes at tidal inlets. These studies should include tracer studies in other important areas of inlet systems such as the deltas and the downdrift beach, as well as the study of the sediment transport pathways under high-energy conditions. The integration of these results into the model would greatly improve its accuracy and applicability, namely for the validation of numerical models.

Acknowledgements

The authors would like to acknowledge all of the collaborators and friends from the University of Algarve that helped us in the experiments and posterior analyses, in particular: Miguel Castro, Patrícia Silva, Rui Santos, Zé Bento and Zé António. Special thanks are given to all of the INDIA fieldwork team that helped in the experiments (especially the Amsterdam, Plymouth and Bordeaux teams). The Dutch team from the University of Amsterdam collected and processed the wind data used for this study, thank you to Bas Arens, John van Boxel, Roos Haring, Robert and Axel. Thanks also to Brad Morris and Rui Taborda for his comments and suggestions. Wave data from the Triaxys buoy were processed at BODC and are part of the INDIA data base. Wave data from the IH were processed by the IH team and are also part of the INDIA data base. Thanks are also given to Havana Bar for providing a nice meeting room during the fieldwork. This work has been partially supported by the following projects: INDIA (INlet Dynamics Initiative Algarve) funded by the commission of the European Directorate General for Science, Research and development under contract MAST3-CT97-0106; CROP (Cross-shore processes in contrasting environments) funded by the Fundação para a Ciência e a Tecnologia de Portugal; Monitorização das Barras do Ancão e da Fuzeta funded by the Instituto de Conservação da Natureza de Portugal. Thanks are given to the Ria Formosa Natural Park for providing the authorisations for the fieldwork campaigns. This work represents contribution n A231 to the Grupo DISEPLA. The authors also acknowledge the help and very useful

suggestions given by Dr. J.T. Wells (Editor of Marine Geology) and two anonymous reviewers that greatly improved this paper.

Appendix A

Notation

A_{Ri}	area represented by each sampling point
d	distance between the FT injection point and the location of the FT_C
d_L	distance between the injection point and the FT_{CL}
F_{mi}	multiplying factor used to extrapolate the results of a sample to the entire represented area
FT	fluorescent tracers
FT_C	total cloud centroid (vertical integration of FT_{CL})
FT_{CL}	FT cloud centroid for each layer
$FT_{injected}$	mass of FT that was injected in the study area
h	height of the samples
H_s	significant wave height
L_1	loss of sediments after one tidal cycle, $t=1$
L_2	losses of sediment at $t=2$
L_{2B}	losses of sediment due to the reworking from sector B
L_{2C}	losses of sediment due to the reworking from sector C
L_{2D}	losses of sediment due to the reworking from sector D
M_{2C}	mass of sediment that is reworked from sector C for stage 2 of the model
M_{2D}	mass of sediment that is reworked from sector D for stage 2 of the model
M_A	known mass of sediment arriving at the western limit of the swash platform at $t=0$
M_i	mass of remaining FT in each representative area
M_L	mass of remaining FT for each layer
M_{Si}	mass of FT found in each sample
M_T	total mass of FT remaining in the study area
MWD	mean wave direction at peak frequency
n	number of FT grains found in each sample
PRFT	percentage of remaining FT
$PRFT_1$	percentage of remaining FT at $t=1$
$PRFT_2$	percentage of remaining FT at $t=2$
Q	sediment transport rate
r	radius of the sample (corer or container)
SB_1	percentage of remaining FT in sector B at $t=1$
SB_2	percentage of remaining FT in sector B at $t=2$
SC_1	percentage of remaining FT in sector C at $t=1$
SC_2	percentage of remaining FT in sector C at $t=2$
SD_1	percentage of remaining FT in sector D at $t=1$
SD_2	percentage of remaining FT in sector D at $t=2$
t	time
T_p	peak period
$\tan \beta_{bf}$	profile slope for the beach face
$\tan \beta_{sp}$	profile slope for the swash platform
V_{FT}	average grain volume of the FT
$V(FT_C)$	total velocity of the FT_C
$V(FT_{CL})$	velocity of displacement of the tracer centroid for each layer
V_{Ri}	representative volume for each sample
V_S	sample volume
X_i	X coordinate for each sampling point
$X(FT_C)$	X coordinate for FT_C
$X(FT_{CL})$	X coordinate for FT_{CL}
Y_i	Y coordinate for each sampling point
$Y(FT_C)$	Y coordinate for FT_C
$Y(FT_{CL})$	Y coordinate for FT_{CL}
Z_o	thickness of the active layer (area given by the average cross-shore profile of mixing depth)
Z_{oi}	mixing depth for each corer sample
ϵ	surf scaling parameter
ξ_b	surf similarity parameter
ρ_s	sand density

References

Allen, J.R., 1988. Nearshore sediment transport. Geogr. Rev. 78 (2), 148–157.

Andrade, C.F., 1990. O Ambiente Barreira da Ria Formosa. PhD Thesis, Univ. Lisboa. 627 pp. (in Portuguese).

Balouin, Y., Howa, H., Michel, D., 2001. Swash platform morphology in the ebb-tidal delta of the Barra Nova Inlet, South-Portugal. J. Coast. Res. 17 (4), 784–791.

Battjes, J.A., 1974. Surf similarity. Proc. Conf. Coastal Engineering'74. ASCE, Honolulu, Hawaii, pp. 466–480.

Bettencourt, P., 1994. Les Environnements Sedimentaires de la Côte Sotavento (Algarve, Sud Portugal) et leur Évolution Holocéne et Actuelle., Univ. Bordeaux I, unpublished. (In French).

Blott, S.J., Pye, K., 2001. Gradistat: a grain size distribution and statistics package for the analysis of unconsolidated sediments. Earth Surf. Process. Landf. 26, 1237–1248.

C.E.R.C., 1984. Shore Protection Manual, 4th ed. Coastal engineering research unit, Dept. of the Army, Washington, DC (354 pp.).

Ciavola, P., 1999. Sediment Transport Processes on Reflective Beaches: Field Experiments in the Algarve. PhD Thesis, Univ. Algarve. 164 pp.

Ciavola, P., Taborda, R., Ferreira, Ó., Dias, J.A., 1997. Field measurements of longshore sand transport and control processes on a steep meso-tidal beach in Portugal. J. Coast. Res. 13 (4), 1119–1129.

Ciavola, P., Dias, N., Ferreira, Ó., Taborda, R., Dias, J.M.A., 1998. Fluorescent sands for measurements of longshore transport rates: a case study from Praia de Faro in southern Portugal. Geo-Mar. Lett. 18, 49–57.

Collins, M.B., Simwell, S.J., Gao, S.S., Powell, H., Hewitson, C., Taylor, J.A., 1995. Water and sediment movement in the vicinity of linear sandbanks: the Norfolk Banks, southern North Sea. Mar. Geol. 123, 125–142.

Costa, C., 1994. Final Report of Sub-Project A. Wind Wave Climatology of the Portuguese Coast. Report PO-WAVES 6/94-A. IH/LNEC. 80 pp.

Dias, J.A., Ferreira, Ó., Matias, A., Vila-Concejo, A., Sá-Pires, C., 2003. Evaluation of soft protection techniques in barrier islands by monitoring programs: case studies from Ria Formosa (Algarve-Portugal). J. Coast. Res. SI (35), 117–131.

Dyer, K.R., Huntley, D.A., 1999. The origin, classification and modelling of sand banks and ridges. Cont. Shelf Res. 19, 1285–1330.

Ferreira, Ó., Fachin, S., Coli, A., Taborda, R., Dias, J.M.A., Lontra, G., 2002. Study of a harbour infilling using sand tracer experiments. Proc. International Coastal Symposium, 25th–29th March 2002, Templepatrick, Northern Ireland. J. Coast. Res., vol. SI (36), pp. 283–289.

FitzGerald, D.M., Buynevich, I.V., Fenster, M.S., McKinlay, P.A., 2000. Sand dynamics at the mouth of a rock-bound, tide-dominated estuary. Sediment. Geol. 131, 25–49.

FitzGerald, D.M., Kraus, N.C., Hands, E.B., 2001. Natural mechanisms of sediment bypassing at tidal inlets. ERDC/CHL CHETN-IV-30, U.S. Army Engineer Research and Development Center, Vicksburg, MS. 10 pp.

Folk, R.L., Ward, W.C., 1957. Brazos River Bar: a study in the significance of grain size parameters. J. Sediment. Petrol. 27 (1), 3–26.

Granja, H., Froidefrond, J.M., Pera, T., 1984. Processus d'evolution morpho-sedimentaire de la Ria Formosa (Portugal). Bull. Inst. Geol., vol. 36. Bassin d'Aquitaine, Bordeaux, pp. 37–50 (in French).

Guza, R.T., Inman, D.L., 1975. Edge waves and beach cusps. J. Geophys. Res. 93, 9302–9314.

Hicks, D.M., Hume, T.M., 1997. Determining sand volumes and bathymetric change on an ebb-tidal delta. J. Coast. Res. 13 (2), 407–416.

Hoyt, J.H., 1967. Barrier island formation. Geol. Soc. Amer. Bull. 78 (9), 1125–1135.

Johnsen, C.D., Cleary, W.J., Freeman, C.W., Sault, M., 1999. Inlet induced shoreline changes, high energy flank of the Cape Fear foreland, SE; NC. Proc. Coastal Sediments '99 Conf.. ASCE, New York, USA, pp. 1402–1417.

Kana, T.W., Mason, J.E., 1988. Evolution of an ebb tidal-delta after an inlet relocation. Lect. Notes Coast. Estuar. Stud. 29, 382–409.

Kamphuis, J.W., Davies, M.H., Nairn, R.B., Sayao, O.J., 1986. Calculation of littoral sand transport rate. Coast. Eng. 10, 1–21.

Komar, P.D., 1977. Selective longshore transport rates of different grain-size fractions within a beach. J. Sediment. Petrol. 47, 1444–1453.

Komar, P.D., Inman, D.L., 1970. Longhore sand transport on beaches. J. Geophys. Res. 75, 5514–5527.

Kraus, N.C., 1985. Field experiments on vertical mixing of sand in the surf zone. J. Sediment. Petrol. 55 (1), 3–14.

Kraus, N.C., Isobe, M., Igarashi, H., Sasaki, T.O., Horikawa, K., 1982. Field experiments on longshore sand transport in the surf zone. Proc. Conf. in Coastal Engineering'82, ASCE, Cape Town, South Africa, pp. 969–988.

Madsen, O.S., 1987. Use of tracers in sediment transport studies. Proc. of Conf. in Coastal Sediments, 1987. ASCE, New Orleans, LA, USA, pp. 424–435.

Michel, M.D., 1997. Evolution Morphodynamique d'un Littoral Sableux Situe a l'Aval d'une Embochadure Lagunaire. PhD Thesis, Univ. Bordeaux I. 162 pp. In French.

Militello, A., Hughes, S.A., 2000. Circulation Patterns at Tidal Inlets with Jetties. ERDC/CHL CETN-IV-29, U.S. Army Engineer Research and Development Center, Vicksburg, MS. 10pp.

Morang, A., 1999. Shinnecock Inlet, New York, Site Investigation: Report 1. Morphology and Historical Behavior. Technical Report CHL-98-32, U.S. Army Engineer Waterways Experiment Station, Vicksburg, MS. 94 pp.

Morris, B.D., Davidson, M.A., Huntley, D.A., 2001. Measurements of the response of a coastal inlet using video monitoring techniques. Mar. Geol. 175, 251–272.

Morris, B.D., Davidson, M.A., Huntley, D.A., 2004. Estimates of the seasonal morphological evolution of the Barra Nova Inlet using video techniques. Cont. Shelf Res. 24/2, 263–278.

Nummedal, D., Fisher, I.A., 1978. Process–response models for depositional shorelines: the German and the Georgia bights. Proc. 16th Coastal Engineering Conf. ASCE, New York, USA, pp. 1215–1231.

O'Connor, B.A., Pan, S., Heron, M., Williams, J.J., Voulgaris, G., Silva, A., 2000. Hydrodynamic modelling of a dynamic inlet. Coast. Eng. 2000 (4), 3472–3481.

Oertel, G.F., 1972. Sediment transport of estuary entrance shoals and the formation of swash platforms. J. Sediment. Petrol. 42 (4), 857–863.

Pessanha, L.E.V., Pires, H.O., 1981. Elementos Sobre o Clima de Agitação Marítima na Costa sul do Algarve. Internal Report Instituto Nacional de Meteorologia e Geofísica 66 pp. In Portuguese.

Pilkey, O.H., Neal, W.J., Monteiro, J.H., Dias, J.M.A., 1989. Algarve barrier islands: a noncoastal-plain system in Portugal. J. Coast. Res. 5 (2), 239–261.

Rosati, J.D., Kraus, N.C., 1999. Advances in coastal sediment budget methodology—with emphasis on inlets. Shore Beach 67 (2 and 3), 56–65.

Smith, J.B., FitzGerald, D.M., 1994. Sediment transport patterns at the Essex river inlet ebb-tidal delta, Massachusetts, USA. J. Coast. Res. 10 (3), 752–774.

Vila, A., Dias, J.M.A., Ferreira, Ó., Matias, A., 1999. Natural Evolution of an Artificial Inlet. Proc. Coastal Sediments '99 Conf. ASCE, New York, USA, pp. 1478–1488.

Vila-Concejo, A., Matias, A., Ferreira, Ó., Duarte, C., Dias, J.M.A., 2002. Recent evolution of the natural inlets of a barrier island system in Southern Portugal. Proc. of International Coastal Symposium, 25th–29th March 2002, Templepatrick, Northern Ireland. J. Coast. Res., vol. SI (36), pp. 741–752.

Vila-Concejo, A., Ferreira, Ó., Matias, A., Dias, J.M.A., 2003a. The first two years of an inlet: sedimentary dynamics. Cont. Shelf Res. 23, 1425–1445.

Vila-Concejo, A., Ferreira, Ó., Ciavola, P., Taborda, R., Dias, J.M.A., 2003b. Quantitative and qualitative analyses of sediment transport paths: straight beaches, inlets and harbours. Proceedings of the International Conference on Coastal Sediments 2003. CD-ROM Published by World Scientific Publishing Corp. and East Meets West Productions, Corpus Christi, Texas, USA. ISBN 981-238-422-7.

Vila-Concejo, A., Ferreira, Ó., Morris, B.D., Matias, A., Dias, J.M.A., 2004. Lessons from inlet relocation: examples from Southern Portugal. Coast. Eng. (in press).

White, T.E., 1998. Status of measurement techniques for coastal sediment transport. Coast. Eng. 35, 17–45.

Williams, G.L., Morang, A., Lillycrop, L., 1998. Shinnecock Inlet, New York, Site Investigation; Report 2, Evaluation of sand bypass options. Technical Report CHL-98-32, U.S. Army Engineer Waterways Experiment Station, Vic.

Williams, J., Arens, B., Aubrey, D., Bell, P., Bizzaro, A., Collins, M., Davidson, M., Dias, J., Ferreira, Ó., Heron, M., Howa, H., Hughes, Z., Huntley, D., Jones, M.T., O'Connor, B., Pan, S., Sarmento, A., Seabra-Santos, F., Shayler, S., Smith, J., Voulgaris, G., 1999. Inlet Dynamics Initiative: Algarve INDIA. Proc. Coastal Sediments '99 Conf. ASCE, New York, USA, pp. 612–627.

Williams, J.J., O'Connor, B.A.O., Arens, S.M., Abadie, S., Bell, P., Balouin, Y., Van Boxel, J.H., do Carmo, A.J., Davidson, M., Ferreira, Ó., Heron, M., Howa, H., Hughes, Z., Kaczmarec, L.M., Kim, H., Morris, B., Nicholson, J., Pan, S., Salles, P., Silva, A., Smith, J., Soares, C., Vila-Concejo, A., 2003. Tidal inlet function: field evidence and numerical simulation in the INDIA project. J. Coast. Res. 19 (1), 189–211.